arXiv:hep-ex/9710012v1 14 Oct 1997

EUROPEAN LABORATORY FOR PARTICLE PHYSICS (CERN)

CERN-PPE/97-128
September 22, 1997

Searches for Charginos and Neutralinos in e^+e^- Collisions at $\sqrt{s} = 161$ and 172 GeV

The ALEPH Collaboration

Abstract

The data recorded by the ALEPH detector at centre-of-mass energies of 161, 170, and 172 GeV are analysed for signals of chargino and neutralino production. No evidence of a signal is found, although candidate events consistent with the expectations from Standard Model processes are observed. Limits at 95% C.L. on the production cross sections are derived and bounds on the parameters of the Minimal Supersymmetric Standard Model are set. The lower limit on the mass of the lightest chargino is 85.5 GeV/c^2 for gaugino-like charginos ($\mu = -500$ GeV/c^2), and 85.0 GeV/c^2 for Higgsino-like charginos ($M_2 = 500$ GeV/c^2), for heavy sneutrinos ($M_{\tilde{\nu}} \geq 200$ GeV/c^2) and $\tan\beta = \sqrt{2}$. The effect of light sleptons on chargino and neutralino limits is investigated. The assumptions of a universal slepton mass and a universal gaugino mass are relaxed, allowing less model-dependent limits to be obtained.

(submitted to Zeitschrift für Physik)

The ALEPH Collaboration

R. Barate, D. Buskulic, D. Decamp, P. Ghez, C. Goy, J.-P. Lees, A. Lucotte, M.-N. Minard, J.-Y. Nief, B. Pietrzyk

Laboratoire de Physique des Particules (LAPP), IN$^2P^3$-CNRS, 74019 Annecy-le-Vieux Cedex, France

M.P. Casado, M. Chmeissani, P. Comas, J.M. Crespo, M. Delfino, E. Fernandez, M. Fernandez-Bosman, Ll. Garrido,[15] A. Juste, M. Martinez, G. Merino, R. Miquel, Ll.M. Mir, C. Padilla, I.C. Park, A. Pascual, J.A. Perlas, I. Riu, F. Sanchez

Institut de Física d'Altes Energies, Universitat Autònoma de Barcelona, 08193 Bellaterra (Barcelona), Spain[7]

A. Colaleo, D. Creanza, M. de Palma, G. Gelao, G. Iaselli, G. Maggi, M. Maggi, N. Marinelli, S. Nuzzo, A. Ranieri, G. Raso, F. Ruggieri, G. Selvaggi, L. Silvestris, P. Tempesta, A. Tricomi,[3] G. Zito

Dipartimento di Fisica, INFN Sezione di Bari, 70126 Bari, Italy

X. Huang, J. Lin, Q. Ouyang, T. Wang, Y. Xie, R. Xu, S. Xue, J. Zhang, L. Zhang, W. Zhao

Institute of High-Energy Physics, Academia Sinica, Beijing, The People's Republic of China[8]

D. Abbaneo, R. Alemany, A.O. Bazarko,[1] U. Becker, P. Bright-Thomas, M. Cattaneo, F. Cerutti, G. Dissertori, H. Drevermann, R.W. Forty, M. Frank, F. Gianotti, R. Hagelberg, J.B. Hansen, J. Harvey, P. Janot, B. Jost, E. Kneringer, I. Lehraus, P. Mato, A. Minten, L. Moneta, A. Pacheco, J.-F. Pusztaszeri,[20] F. Ranjard, G. Rizzo, L. Rolandi, D. Rousseau, D. Schlatter, M. Schmitt, O. Schneider, W. Tejessy, F. Teubert, I.R. Tomalin, H. Wachsmuth, A. Wagner[21]

European Laboratory for Particle Physics (CERN), 1211 Geneva 23, Switzerland

Z. Ajaltouni, A. Barrès, C. Boyer, A. Falvard, C. Ferdi, P. Gay, C . Guicheney, P. Henrard, J. Jousset, B. Michel, S. Monteil, J-C. Montret, D. Pallin, P. Perret, F. Podlyski, J. Proriol, P. Rosnet, J.-M. Rossignol

Laboratoire de Physique Corpusculaire, Université Blaise Pascal, IN$^2P^3$-CNRS, Clermont-Ferrand, 63177 Aubière, France

T. Fearnley, J.D. Hansen, J.R. Hansen, P.H. Hansen, B.S. Nilsson, B. Rensch, A. Wäänänen

Niels Bohr Institute, 2100 Copenhagen, Denmark[9]

G. Daskalakis, A. Kyriakis, C. Markou, E. Simopoulou, A. Vayaki

Nuclear Research Center Demokritos (NRCD), Athens, Greece

A. Blondel, J.C. Brient, F. Machefert, A. Rougé, M. Rumpf, A. Valassi,[6] H. Videau

Laboratoire de Physique Nucléaire et des Hautes Energies, Ecole Polytechnique, IN$^2P^3$-CNRS, 91128 Palaiseau Cedex, France

T. Boccali, E. Focardi, G. Parrini, K. Zachariadou

Dipartimento di Fisica, Università di Firenze, INFN Sezione di Firenze, 50125 Firenze, Italy

R. Cavanaugh, M. Corden, C. Georgiopoulos, T. Huehn, D.E. Jaffe

Supercomputer Computations Research Institute, Florida State University, Tallahassee, FL 32306-4052, USA[13,14]

A. Antonelli, G. Bencivenni, G. Bologna,[4] F. Bossi, P. Campana, G. Capon, D. Casper, V. Chiarella, G. Felici, P. Laurelli, G. Mannocchi,[5] F. Murtas, G.P. Murtas, L. Passalacqua, M. Pepe-Altarelli

Laboratori Nazionali dell'INFN (LNF-INFN), 00044 Frascati, Italy

L. Curtis, S.J. Dorris, A.W. Halley, I.G. Knowles, J.G. Lynch, V. O'Shea, C. Raine, J.M. Scarr, K. Smith, P. Teixeira-Dias, A.S. Thompson, E. Thomson, F. Thomson, R.M. Turnbull

Department of Physics and Astronomy, University of Glasgow, Glasgow G12 8QQ,United Kingdom[10]

O. Buchmüller, S. Dhamotharan, C. Geweniger, G. Graefe, P. Hanke, G. Hansper, V. Hepp, E.E. Kluge, A. Putzer, J. Sommer, K. Tittel, S. Werner, M. Wunsch

Institut für Hochenergiephysik, Universität Heidelberg, 69120 Heidelberg, Fed. Rep. of Germany[16]

R. Beuselinck, D.M. Binnie, W. Cameron, P.J. Dornan, M. Girone, S. Goodsir, E.B. Martin, P. Morawitz,

A. Moutoussi, J. Nash, J.K. Sedgbeer, P. Spagnolo, A.M. Stacey, M.D. Williams

Department of Physics, Imperial College, London SW7 2BZ, United Kingdom[10]

V.M. Ghete, P. Girtler, D. Kuhn, G. Rudolph

Institut für Experimentalphysik, Universität Innsbruck, 6020 Innsbruck, Austria[18]

A.P. Betteridge, C.K. Bowdery, P.G. Buck, P. Colrain, G. Crawford, A.J. Finch, F. Foster, G. Hughes, R.W.L. Jones, T. Sloan, E.P. Whelan, M.I. Williams

Department of Physics, University of Lancaster, Lancaster LA1 4YB, United Kingdom[10]

I. Giehl, C. Hoffmann, K. Jakobs, K. Kleinknecht, G. Quast, B. Renk, E. Rohne, H.-G. Sander, P. van Gemmeren, C. Zeitnitz

Institut für Physik, Universität Mainz, 55099 Mainz, Fed. Rep. of Germany[16]

J.J. Aubert, C. Benchouk, A. Bonissent, G. Bujosa, J. Carr, P. Coyle, C. Diaconu, A. Ealet, D. Fouchez, N. Konstantinidis, O. Leroy, F. Motsch, P. Payre, M. Talby, A. Sadouki, M. Thulasidas, A. Tilquin, K. Trabelsi

Centre de Physique des Particules, Faculté des Sciences de Luminy, IN^{2}P^3-CNRS, 13288 Marseille, France

M. Aleppo, M. Antonelli, F. Ragusa

Dipartimento di Fisica, Università di Milano e INFN Sezione di Milano, 20133 Milano, Italy.

R. Berlich, W. Blum, V. Büscher, H. Dietl, G. Ganis, C. Gotzhein, H. Kroha, G. Lütjens, G. Lutz, W. Männer, H.-G. Moser, R. Richter, A. Rosado-Schlosser, S. Schael, R. Settles, H. Seywerd, R. St. Denis, H. Stenzel, W. Wiedenmann, G. Wolf

Max-Planck-Institut für Physik, Werner-Heisenberg-Institut, 80805 München, Fed. Rep. of Germany[16]

J. Boucrot, O. Callot,[12] S. Chen, M. Davier, L. Duflot, J.-F. Grivaz, Ph. Heusse, A. Höcker, A. Jacholkowska, D.W. Kim,[2] F. Le Diberder, J. Lefrançois, A.-M. Lutz, M. Marumi, M.-H. Schune, L. Serin, E. Tournefier, J.-J. Veillet, I. Videau, D. Zerwas

Laboratoire de l'Accélérateur Linéaire, Université de Paris-Sud, IN^{2}P^3-CNRS, 91405 Orsay Cedex, France

P. Azzurri, G. Bagliesi,[12] S. Bettarini, C. Bozzi, G. Calderini, V. Ciulli, R. Dell'Orso, R. Fantechi, I. Ferrante, A. Giassi, A. Gregorio, F. Ligabue, A. Lusiani, P.S. Marrocchesi, A. Messineo, F. Palla, G. Sanguinetti, A. Sciabà, G. Sguazzoni, J. Steinberger, R. Tenchini, C. Vannini, A. Venturi, P.G. Verdini

Dipartimento di Fisica dell'Università, INFN Sezione di Pisa, e Scuola Normale Superiore, 56010 Pisa, Italy

G.A. Blair, L.M. Bryant, J.T. Chambers, M.G. Green, T. Medcalf, P. Perrodo, J.A. Strong, J.H. von Wimmersperg-Toeller

Department of Physics, Royal Holloway & Bedford New College, University of London, Surrey TW20 OEX, United Kingdom[10]

D.R. Botterill, R.W. Clifft, T.R. Edgecock, S. Haywood, P. Maley, P.R. Norton, J.C. Thompson, A.E. Wright

Particle Physics Dept., Rutherford Appleton Laboratory, Chilton, Didcot, Oxon OX11 OQX, United Kingdom[10]

B. Bloch-Devaux, P. Colas, B. Fabbro, E. Lançon, M.C. Lemaire, E. Locci, P. Perez, J. Rander, J.-F. Renardy, A. Rosowsky, A. Roussarie, J. Schwindling, A. Trabelsi, B. Vallage

CEA, DAPNIA/Service de Physique des Particules, CE-Saclay, 91191 Gif-sur-Yvette Cedex, France[17]

S.N. Black, J.H. Dann, H.Y. Kim, A.M. Litke, M.A. McNeil, G. Taylor

Institute for Particle Physics, University of California at Santa Cruz, Santa Cruz, CA 95064, USA[19]

C.N. Booth, C.A.J. Brew, S. Cartwright, F. Combley, M.S. Kelly, M. Lehto, J. Reeve, L.F. Thompson

Department of Physics, University of Sheffield, Sheffield S3 7RH, United Kingdom[10]

K. Affholderbach, A. Böhrer, S. Brandt, G. Cowan, J. Foss, C. Grupen, L. Smolik, F. Stephan

Fachbereich Physik, Universität Siegen, 57068 Siegen, Fed. Rep. of Germany[16]

M. Apollonio, L. Bosisio, R. Della Marina, G. Giannini, B. Gobbo, G. Musolino

Dipartimento di Fisica, Università di Trieste e INFN Sezione di Trieste, 34127 Trieste, Italy

J. Putz, J. Rothberg, S. Wasserbaech, R.W. Williams

Experimental Elementary Particle Physics, University of Washington, WA 98195 Seattle, U.S.A.

S.R. Armstrong, E. Charles, P. Elmer, D.P.S. Ferguson, Y. Gao, S. González, T.C. Greening, O.J. Hayes, H. Hu, S. Jin, P.A. McNamara III, J.M. Nachtman, J. Nielsen, W. Orejudos, Y.B. Pan, Y. Saadi, I.J. Scott, J. Walsh, Sau Lan Wu, X. Wu, J.M. Yamartino, G. Zobernig

Department of Physics, University of Wisconsin, Madison, WI 53706, USA[11]

---

[1] Now at Princeton University, Princeton, NJ 08544, U.S.A.

[2] Permanent address: Kangnung National University, Kangnung, Korea.

[3] Also at Dipartimento di Fisica, INFN Sezione di Catania, Catania, Italy.

[4] Also Istituto di Fisica Generale, Università di Torino, Torino, Italy.

[5] Also Istituto di Cosmo-Geofisica del C.N.R., Torino, Italy.

[6] Supported by the Commission of the European Communities, contract ERBCHBICT941234.

[7] Supported by CICYT, Spain.

[8] Supported by the National Science Foundation of China.

[9] Supported by the Danish Natural Science Research Council.

[10] Supported by the UK Particle Physics and Astronomy Research Council.

[11] Supported by the US Department of Energy, grant DE-FG0295-ER40896.

[12] Also at CERN, 1211 Geneva 23,Switzerland.

[13] Supported by the US Department of Energy, contract DE-FG05-92ER40742.

[14] Supported by the US Department of Energy, contract DE-FC05-85ER250000.

[15] Permanent address: Universitat de Barcelona, 08208 Barcelona, Spain.

[16] Supported by the Bundesministerium für Bildung, Wissenschaft, Forschung und Technologie, Fed. Rep. of Germany.

[17] Supported by the Direction des Sciences de la Matière, C.E.A.

[18] Supported by Fonds zur Förderung der wissenschaftlichen Forschung, Austria.

[19] Supported by the US Department of Energy, grant DE-FG03-92ER40689.

[20] Now at School of Operations Research and Industrial Engireering, Cornell University, Ithaca, NY 14853-3801, U.S.A.

[21] Now at Schweizerischer Bankverein, Basel, Switzerland.

1 Introduction

In 1996, a new regime in e^+e^- collisions was entered when LEP energies reached and exceeded the W pair production threshold. Data were collected with the ALEPH detector at $\sqrt{s} = 161.3$ GeV (10.8 pb^{-1}), $\sqrt{s} = 170.3$ GeV (1.1 pb^{-1}) and $\sqrt{s} = 172.3$ GeV (9.6 pb^{-1}). The increased centre-of-mass energies motivate the direct search for new physics, in particular for particles predicted by supersymmetric theories.

Supersymmetry (SUSY) [1] requires the number of degrees of freedom associated with the fermionic and bosonic fields of the theory to be the same. This is achieved by augmenting the ordinary field multiplets with additional fields differing by a half unit of spin. The resulting particle spectrum contains several new states: gauginos, associated with the ordinary gauge bosons; Higgsinos with the Higgs bosons; sleptons, sneutrinos and squarks with the ordinary matter fermions. Here, searches for supersymmetric partners of the gauge and Higgs bosons are reported, while searches at these energies for sleptons [2], stops [3] and Higgs bosons [4] have been reported previously. Searches similar to those discussed here have been reported by the OPAL collaboration [5].

The Minimal Supersymmetric Standard Model (MSSM) is the supersymmetric extension of the Standard Model with minimal field content. Two doublets of complex scalar fields are introduced to give mass to the up-like and down-like fermions via the Higgs mechanism. The ratio of the two vacuum expectation values is denoted $\tan\beta$ and the Higgs mass term is μ. Soft SUSY breaking terms lift the mass degeneracy of ordinary particles and their SUSY partners. The scale of these terms should not exceed $\sim$1 TeV/c^2 in order for supersymmetry to remain a solution of the naturalness problem. These SUSY breaking terms are: gaugino masses M_1, M_2 and M_3, associated to the $U(1)$, $SU(2)$ and $SU(3)$ gauge groups, respectively; and mass terms m_i and trilinear couplings A_i for the various sfermions. The partners of the photon, Z and neutral Higgs bosons mix to form four mass eigenstates called neutralinos, $\chi, \chi', \chi'', \chi'''$, in order of increasing mass. Similarly, charged gauginos ($\widetilde{\mathrm{W}}^+$) and Higgsinos ($\widetilde{\mathrm{H}}^+$) form charginos, $\chi^\pm$ and $\chi_2^\pm$. Ordinary particles and supersymmetric particles are distinguished by their R-parity, a multiplicative quantum number, which is assumed to be conserved to ensure lepton and baryon number conservation. As a consequence, supersymmetric particles are produced in pairs and decay to the Lightest Supersymmetric Particle (LSP), assumed here to be the lightest neutralino, which is weakly interacting and does not decay, escaping detection.

The large number of free parameters in the MSSM can be reduced by making certain theoretical assumptions. First, the gaugino masses may be assumed to unify at the GUT scale, leading, at the electroweak scale, to the relation: $M_1 = \frac{5}{3}\tan^2\theta_W\ M_2$. Second, the masses of the sleptons might also unify at the GUT scale with value m_0. Their masses at the electroweak scale are derived using the renormalization group equations [6], and are an increasing function of m_0. These assumptions are made for many of the results presented here. A special effort is made to interpret the results within a larger framework, relaxing the gaugino mass and/or the scalar mass unification assumptions.

Given the large value of the top quark mass [7], the "infrared quasi fixed point scenario" [8] favours low ($\tan\beta{\sim}1-3$) or high ($\tan\beta{\sim}30$) values of $\tan\beta$. The various selections are optimised for a value of $\tan\beta$ equal to $\sqrt{2}$, typical of the low $\tan\beta$ solution. Unless otherwise specified, the results are presented for that same value of $\tan\beta$. High $\tan\beta$ values tend to give stronger constraints.

With unification of gaugino mass terms, in the region where $M_2 \gg |\mu|$ the lightest chargino and neutralino have large Higgsino components; this is referred to as the "Higgsino" region. Here, the lightest neutralino χ is generally close in mass to the lightest chargino and to the second lightest neutralino. Similarly, the region where $|\mu| \gg M_2$ is referred to as the "gaugino" region; here, $M_\chi \simeq M_{\chi^\pm}/2$. In both regions, $M_{\chi'} > M_{\chi^\pm}$. In the region of small negative μ and low M_2, one of the two lightest neutralinos has large gaugino components, while the other has large Higgsino components. The chargino has sizeable gaugino and Higgsino components. This region will be referred to as the "mixed" region.

At LEP, charginos are pair produced by virtual photon or Z exchange in the s channel, and sneutrino exchange in the t channel [9]. The s and t channels interfere destructively, so that low sneutrino masses lead to smaller cross sections. Neutralinos are produced by s-channel Z exchange and t-channel selectron exchange [10]. Here, the s and t channels interfere constructively for most of the parameter space. As a consequence, cross sections are usually higher if selectrons are light.

Charginos decay to a neutralino and a lepton-neutrino or quark-antiquark pair. If all sfermions are heavy (large m_0), the decay proceeds mainly through the exchange of a virtual W. The dominant final state topologies for chargino pair production are then hadronic events with missing energy carried away by the two neutralino LSP's, called here the four-jet topology (4J), or events with hadrons, an isolated lepton and missing energy (2JL topology). Acoplanar lepton pairs (AL topology) are also produced, but at a much lower rate. The second lightest neutralino χ' decays to a neutralino and a fermion-antifermion pair. If all sfermions are heavy, the decay proceeds mainly through the exchange of a virtual Z. The main final state resulting from $\chi\chi'$ production therefore consists of acoplanar jets (AJ), due to the small Z leptonic branching ratio. (The $\chi\chi$ final state is invisible.)

Selections for the 4J, 2JL and AJ topologies are designed for chargino and neutralino masses close to the kinematic limit for $\chi^+\chi^-$ or $\chi\chi'$ production and are optimised for decays dominated by W* (Z*) exchange and for various ΔM ranges. Here ΔM is the mass difference between the lightest neutralino and the chargino or the second lightest neutralino. The signal properties, and hence the background composition and significance, change dramatically with the mass difference: for low ΔM, the phase space for decay is small and the signal topology resembles that of $\mathrm{e^+e^- \to e^+e^- f\bar{f}}$ events, while for very large ΔM, as is the case for massless neutralinos, the signal for chargino production is more WW-like. Small mass differences are typical of the Higgsino region while large mass differences correspond to the gaugino and mixed regions.

When sleptons are light, leptonic chargino and neutralino decays are enhanced, due to the increased influence of slepton exchange diagrams. Since no signal for squarks has been found at the Tevatron [11], their masses should be heavy enough to make any influence on chargino and neutralino decays negligible. On the contrary, sleptons are expected to be lighter due to smaller radiative corrections to their masses; hence light slepton effects on the leptonic branching ratios of charginos and neutralinos can not be neglected. The dominant topologies are then acoplanar lepton pairs, and the selections are based on those designed for the slepton searches [2]. When sleptons are light enough, two-body decays such as $\chi^\pm \to l\tilde{\nu}$ or $\chi' \to \nu\tilde{\nu}$ open up, the latter leading to an invisible final state.

In the Higgsino region, $\chi\chi'$ production is the only relevant neutralino process. In the mixed region, the heavier neutralinos χ'' and χ''' can also be produced. Complex topologies arising from cascade and radiative decays are covered by a few dedicated searches.

In the various selections, the cuts are adjusted according to the "$\bar{N}_{95}$ prescription" [12]. The optimal compromise between signal efficiency and background level is obtained when the expected 95% C.L. upper limit on the cross section is minimised based on Monte Carlo simulations; this optimum changes, *i.e.*, the cuts become tighter, as the integrated luminosity increases. The $\gamma\gamma \to hadrons$ background is handled differently, due to the difficulties to model this process and to simulate the detector response at the level of accuracy imposed by its large cross section. In this case, more severe criteria are applied than would result from the $\bar{N}_{95}$ procedure, as explained in Section 3.2. For any given chargino and neutralino mass combination (or any choice of M_2, μ and $\tan\beta$) and for any given leptonic branching ratio (or any choice of m_0), an optimal combination of the various selections is chosen, again according to the $\bar{N}_{95}$ prescription, counting events that pass any of the combined selections to determine efficiencies and contaminations.

In the specific case of large slepton masses, the selection efficiency for chargino pair production depends mostly on the chargino and neutralino masses. Therefore, results can be presented not only in the MSSM parameter space but also in terms of limits on the chargino pair production cross section as a function of these two masses in a fairly general way. A similar statement holds for $\chi\chi'$ production (neglecting possible $\chi' \to \chi\gamma$ decays at this stage). To take into account in a consistent way the other neutralino production channels, such as $e^+e^- \to \chi'\chi''$, and also to cope with lower m_0 values, the validity of the MSSM with all the unification conditions mentioned earlier is assumed. Because of possible large mixing in the stau sector, three-body decays involving taus can dominate over those involving other lepton flavours, and the two-body decay $\chi^\pm \to \tilde{\tau}\nu$ may open up before $\chi^\pm \to l\tilde{\nu}$. Attention is given to those possibilities. The dependence of the results on the assumption of universality of scalar masses and gaugino masses is investigated.

The outline of this paper is as follows: after a brief description of the ALEPH detector in Section 2, the various selections are detailed in Section 3, the results and their interpretation are presented in Section 4 and conclusions are drawn in Section 5.

2 The ALEPH Detector

The ALEPH detector is described in detail in [13] and its performances in [14]; only the features most relevant for the chargino and neutralino analyses are given here.

The detector is required to be fully operational. At least one of the major triggers for supersymmetry searches (total energy triggers, single charged electromagnetic and single muon triggers [13]) is required to be fired.

Charged particle tracks are measured by a silicon vertex detector, a drift chamber and a large time projection chamber (TPC), immersed in a 1.5 Tesla magnetic field provided by a superconducting magnet. A momentum resolution up to $\Delta P_T/P_T = 6 \times 10^{-4} P_T + 0.005$ (P_T in GeV/c) can be achieved.

The electromagnetic calorimeter (ECAL), a sandwich of lead sheets and proportional tubes, is located inside the coil. Highly granular transverse and longitudinal measurements of electromagnetic showers are provided by projective towers, which are segmented longitudinally in three storeys. The achieved energy resolution is $\Delta E/E \simeq 18\%/\sqrt{E} + 0.009$ (E in GeV). The ECAL angular coverage extends down to within 10° from the beam axis.

The iron return yoke is instrumented as a hadron calorimeter (HCAL) consisting of projective towers giving a measurement of the shower energy. The pattern of fired streamer tubes provides a two-dimensional view of the energy deposit, which is useful for identifying muons. The HCAL covers polar angles down to $\theta = 8°$. Streamer chambers outside of the HCAL ("muon chambers") are used to tag penetrating charged particles.

The calorimetric coverage is extended down to polar angles of 24 mrad by the luminosity calorimeters LCAL and SICAL. The low-angle acceptance of SICAL, below 34 mrad, is shadowed by a shielding mask installed in 1996 to reduce the potentially higher machine background at LEP2.

As the main signal for the processes searched here is missing energy, a good hermiticity of the detector is essential. The ECAL and HCAL cracks are not aligned, so there are no acceptance holes in ALEPH at large polar angles. The HCAL covers the gap between the ECAL and the LCAL so particles originating from the interaction point passing through this gap are detected. The LCAL consists of two half modules on each side of the detector, with a small vertical inactive region. This crack is partially covered by HCAL.

The information from the tracking detectors and the calorimeters is combined by an energy flow algorithm described in [14]. For each event, a list of energy flow objects (charged particles, photons, neutral hadrons, clusters in the luminosity calorimeters) is provided. The analyses presented here are based on these objects such that, for example, the visible mass is the invariant mass of all objects and the P_T is the component transverse to the beam axis of the momentum sum of all objects.

Lepton identification is described in [14]. Electrons are identified using their specific ionisation in the TPC ($\mathrm{d}E/\mathrm{d}x$) and the transverse and longitudinal shower shapes in ECAL. Muons are separated from hadrons by their characteristic penetrating pattern in HCAL and the presence of hits in the muon chambers.

3 Searches for Charginos and Neutralinos

The various selections for chargino and neutralino searches are presented in this section. The chargino analyses in the 4J and 2JL topologies are designed for four ΔM regions: very low (VL) for $\Delta M \simeq 5$ GeV/c^2, low (L) for $\Delta M \simeq 10$ GeV/c^2, high (H) ($\Delta M \simeq M_{\chi^+}/2$) and very high (VH) ($\Delta M \simeq 80$ GeV/c^2). Two neutralino analyses in the AJ topology (AJ-L and AJ-H) are designed for ΔM smaller than or greater than 30 GeV/c^2. Additional selections address the acoplanar lepton pair topology and the more complex final states encountered in the neutralino searches.

The 4J-VH and 2JL-VH chargino selections are optimised separately for $\sqrt{s} = 161$ GeV and $\sqrt{s} = 172$ GeV, due to a large increase in the WW cross section, which is the most difficult background for this range of ΔM. In the other chargino and neutralino selections, a single set of cuts is applied for the two energies; this does not degrade the performance of the analyses at either energy. Although the selections can be optimised for a given ΔM, in general they are not optimal when ΔM is changed by a small amount. In order to maintain a smooth transition between the various ΔM regions in the chargino analysis (VH, H, L, VL), each selection is optimised on a signal containing an admixture of the nearby ΔM configurations, typically weighting by 50% a configuration at the midpoint of the ΔM range, $\overline{\Delta M}$, and 25% each at $\Delta M = \overline{\Delta M} \pm 20$ GeV/c^2. The optimisation procedure is performed by means of a program that varies all cuts simultaneously, in order to take correlations between variables into account.

In the following, the various Monte Carlo samples used for selection optimisation are described first. The specific criteria applied to reject the $\gamma\gamma \to$ *hadrons* background are addressed next.

The searches for charginos are then described, followed by the searches for neutralinos. The combinations of selections applied in the various cases are presented, and the corresponding search efficiencies are given. A discussion of the systematic errors follows.

3.1 Monte Carlo Sample

The Monte Carlo generator DFGT [15] is used to simulate the chargino events. This generator takes into account the spin correlation in the production and decay of charginos. The final states are interfaced for the hadronisation process to JETSET 7.4 [16] and initial state radiation is included.

Another widely used generator for supersymmetry is SUSYGEN [17] which simulates the production and decays of charginos, neutralinos, sleptons and squarks, including cascade decays. It is used for neutralino production and as a cross-check for chargino production. Final state radiation is taken into account using PHOTOS [18].

Dilepton Standard Model processes are simulated with KORALZ [19] for $\mu^+\mu^-$ and $\tau^+\tau^-$ and UNIBAB [20] for Bhabha production. KORALW [21] is used to generate W-pair events. Leptonic two-photon events are generated with PHOT02 [22]. PYTHIA [23] is used to generate $\gamma\gamma \to$ *hadrons* events. This generator is restricted to "untagged" events where the outgoing electrons are nearly undeflected. The PYTHIA sample is complemented by events generated with PHOT02 where an electron is required to be deflected by at least 5 mrad. The $\gamma\gamma$ events are generated with an invariant mass cut of 3.5 GeV/c^2. All other processes ($q\bar{q}\gamma$, ZZ, Weν and Zee) are generated using PYTHIA, with an invariant mass cut for the resonance of 0.2 GeV/c^2 for ZZ and Weν and 2 GeV/c^2 for Zee. Here, "Z" also includes Z* and γ^* production. Samples corresponding to at least 20 times the integrated luminosity of the data are generated, except for $\gamma\gamma \to$ *hadrons*. This process is simulated with three times the integrated luminosity of the data, only for 161 GeV because of the slow dependence of the event properties on $\sqrt{s}$.

3.2 Rejection of $\gamma\gamma \to$ hadrons

The $\gamma\gamma \to$ *hadrons* background is particularly important for the VL and L mass difference regions but may also contaminate other analyses due to its large cross-section ($\sim$ 13 nb). First the strategy and the variables used for the rejection of this background are presented, then the specific cuts for each chargino and neutralino selection are discussed.

3.2.1 Strategy

Transverse momentum is the most natural quantity to reject this background. For an ideal detector covering the solid angle above 34 mrad with unlimited precision, requiring the event transverse momentum P_T to be in excess of 3 $\%\sqrt{s}$ should reject all the $\gamma\gamma \to$ *hadrons* events. Unfortunately, the measurement of the visible system is not ideal and fluctuations can induce "fake" P_T; hence rejection of events with some energy at low angle is needed. However, the energy veto may be rendered ineffective by inactive regions, such as the vertical LCAL crack; new variables, discussed in the next section, are therefore needed to detect these situations. Furthermore, the Monte Carlo prediction for this background suffers from detector simulation problems and from inaccuracy in the simulation of the underlying physics.

Due to these potential problems, energy-based quantities are used in conjunction with quantities based on direction measurements to ensure a better rejection of $\gamma\gamma$ events. Any event that is rejected by only one cut is still counted as a fraction of an event in the background estimation, the exact value depending on how far away the cut variable for this event is from the cut value, taking into account the distribution of the variable as well as its sensitivity to reconstruction problems.

3.2.2 Variables

Due to the simple kinematics of $\gamma\gamma$ events, it is possible to reconstruct the four-momentum of the outgoing deflected electron (positron) from the properties of the event, assuming that the outgoing positron (electron) is not deflected at all ($\theta = 0°$). The scattering angle θ_{scat} is defined to be the minimum polar angle of the deflected particle for the two hypotheses. The pointing angle θ_{point} is the minimum angle between the calculated deflected particle and any energy flow object. In $\gamma\gamma$ events, for large enough θ_{scat}, the outgoing particle should be visible. Even if only a fraction of its energy is detected, *e.g.* due to cracks, θ_{point} should be small, as the reconstructed particle will "point" to the energy deposits.

The acoplanarity ($\Delta\phi$) is the azimuthal angle between the momentum sum of particles in each hemisphere of an event, defined by a plane perpendicular to the thrust axis. Due to the large missing momentum along the beam axis in $\gamma\gamma$ events, the transverse acoplanarity is introduced. It is calculated by first projecting the event onto the plane perpendicular to the beam axis, calculating the two-dimensional thrust axis and dividing the event into two hemispheres by a plane perpendicular to this thrust axis. The transverse acoplanarity $\Delta\phi_{\text{T}}$ is the angle between the two hemisphere momentum sums.

Since the visible energy is small in $\gamma\gamma$ events, the kinematics of the event can be distorted by minor reconstruction problems. In particular, fake neutral hadrons are created when the energy deposit of a charged particle in the calorimeters is not associated with its reconstructed track. To cope with such events, the fraction of the visible energy carried by neutral hadrons ($F_{NH} = E_{NH}/E_{\text{vis}}$) as well as the P_T of the event excluding neutral hadrons from its calculation ($P_T^{\overline{NH}}$) are used.

3.2.3 Common cuts

Monte Carlo $\gamma\gamma$ events are generated with an invariant mass of the hadronic system greater than 3.5 GeV/c^2; thus, in all analyses, the visible mass is required to be greater than 4 GeV/c^2.

With the required set of triggers, trigger inefficiency is not negligible for $\gamma\gamma$ events nor for signal events in the very low ΔM region, but is small for events that would have been selected by any of the selections described hereafter. The most important triggers for $\gamma\gamma$ events rely on the energy measurement in ECAL. It has been checked that the Monte Carlo reproduces well the energy distribution except for the threshold behaviour; in order to avoid that potentially dangerous region, higher trigger thresholds are applied offline on data and Monte Carlo events.

The cuts designed to eliminate the $\gamma\gamma \to \textit{hadrons}$ background for the very high, high and low mass difference chargino analyses and for neutralino analyses are detailed here and summarised in Table 1. Specific analyses, described in Section 3.3, are designed in the very low ΔM case, where the main background is $\gamma\gamma \to \textit{hadrons}$.

3.2.4 Rejection of $\gamma\gamma \rightarrow$ hadrons in the chargino selections

Four Jet Topology (4J) For the 4J-VH and 4J-H selections, the number of good charged tracks is required to exceed six. The event *thrust* must not exceed 0.9. The P_T is required to be larger than $5\%\sqrt{s}$ or $7.5\%\sqrt{s}$ if the azimuthal angle of the missing momentum ϕ_{miss} is within 15° of the vertical plane. Although the actual size of the LCAL vertical crack is much smaller than 15°, the angular region that defines it must take into account the resolution on the missing momentum direction. The transverse acoplanarity must be less than 175°. The energy detected within 12° of the beam axis, E_{12}, must be lower than $5\%\sqrt{s}$ and θ_{scat} must be greater than 15° or θ_{point} must be greater than 5°. The missing momentum is required to point at least 18.2° away from the beam axis ($|\cos\theta_{\text{miss}}| < 0.95$). To reject events with fake neutral hadrons, F_{NH} must be lower than 30%. This cut is relaxed to 45% if $P_T^{\overline{NH}}$ is greater than $3\%\sqrt{s}$. Finally, to avoid large angle tagged $\gamma\gamma$ events, the energy of the most energetic lepton of the event must not exceed $20\%\sqrt{s}$.

For the 4J-L chargino analysis, at least four good tracks must be reconstructed. All cuts defined above are applied, with the exception of the *thrust* cut. In addition, E_{12} must be zero and the θ_{point} cut is tightened to 10°. Finally, the energy in a 30° azimuthal wedge around the direction of the missing momentum (E_{w}^{30}) must not exceed $1.5\%\sqrt{s}$.

Two Jets and Lepton Topology (2JL) The rejection of the $\gamma\gamma$ background in the 2JL selections is easier due to the presence of an identified lepton. An electron (muon) of at least 2 GeV (2.5 GeV) must be identified. The number of charged tracks (including the lepton) must be at least three and $\Delta\phi_{\text{T}}$ lower than 175°. θ_{scat} must be greater than 15° or θ_{point} greater than 5°. The neutral hadron energy fraction is required to be less than 45%. In the 2JL-VH and 2JL-H selections, the P_T and E_{12} cuts are the same as for the 4J-H channel. In the 2JL-H selection, the energy of the most energetic lepton must be less than $20\%\sqrt{s}$. This cut would greatly reduce the efficiency for the 2JL-VH selection, and is relaxed to $30\%\sqrt{s}$; in addition, the missing mass M_{miss} is required to be greater than $25\%\sqrt{s}$. In the 2JL-L analysis, the P_T must exceed $2.5\%\sqrt{s}$, E_{12} must be zero and $|\cos\theta_{\text{miss}}| < 0.95$. The energy in a cone of 30° around the most energetic lepton in the event (E_{ℓ}^{30}) is calculated, and E_{ℓ}^{30} or E_{w}^{30} must be lower than $1\%\sqrt{s}$.

No events from the various $\gamma\gamma \rightarrow$ *hadrons* Monte Carlo samples survive the 4J and 2JL selection cuts and none are rejected by only one cut. For the double rejection requirement, the P_T cut is reinforced by the $\Delta\phi_{\text{T}}$ cut and by the F_{NH} and $P_T^{\overline{NH}}$ cuts in the case of fake neutral hadrons. The E_{12} and pointing (θ_{scat} and θ_{point}) cuts reinforce each other (see Table 1).

3.2.5 Rejection of $\gamma\gamma \rightarrow$ hadrons in the neutralino AJ selections

In the neutralino AJ selections, the cuts on $|\cos\theta_{\text{miss}}|$, E_{12}, E_{ℓ}, θ_{point} and θ_{scat} are the same as in the 4J-H analysis. The neutral hadron energy is required to be less than 45% of the visible energy. In the AJ-L analysis, at least four good tracks must be reconstructed in the event and the P_T is required to exceed $3\%\sqrt{s}$ ($4.5\%\sqrt{s}$ if ϕ_{miss} is within 15° of the vertical plane). The transverse acoplanarity is required to be smaller than 120°. E_{12} and E_{w}^{30} must be equal to zero. The P_T is required to be larger than 40% of the visible energy, and F_{NH} less than 30% unless $P_T^{\overline{NH}}$ is greater than $1.8\%\sqrt{s}$. In the AJ-H analysis, the number of good tracks must be larger than six and the acoplanarity and transverse acoplanarity must be smaller than 175°. The P_T is required to exceed $5\%\sqrt{s}$ ($7.5\%\sqrt{s}$ if ϕ_{miss} is within 15° of the vertical plane) and also to be larger than 20% of the visible energy. The cuts on F_{NH} and E_{12} are the same as in the 4J-H analysis. Finally the fraction of visible energy within 30° of the beam axis E_{30° is required to be less than 70%, and $E_{\rm w}^{30}$ less than $7.5\%\sqrt{s}$.

All Monte Carlo $\gamma\gamma \to$ *hadrons* events are eliminated by at least two cuts in the AJ-H analysis. In the AJ-L analysis, the $\gamma\gamma \to$ *hadrons* background is estimated to be $\simeq$20 fb from the distance to the cut values of a few singly cut events.

3.3 Chargino selections

There are three topologies for chargino searches: a totally hadronic topology (4J), a topology with a lepton and jets (2JL) and a topology of two acoplanar leptons (AL), not necessarily of the same flavour. Several analyses are employed in each topology to provide sensitivity over a large range of mass differences (very high, high, low and very low ΔM). The criteria for the rejection of the $\gamma\gamma \to$ *hadrons* background have been described in the previous Section.

Four-Jet Topology (4J) The most important backgrounds for 4J-VH and 4J-H are $q\bar{q}\gamma$ and WW production. The missing transverse momentum P_T, the transverse imbalance $P_T/E_{\rm vis}$ (see Fig. 1a), the visible mass $M_{\rm vis}$ and the acoplanarity are used to reduce these backgrounds. No explicit reconstruction of four jets is made but the event should be spherical (using the *thrust* or the inverse-boost: $Inv\mathcal{B} = \sqrt{\frac{1}{2}(1/\gamma_1^2 + 1/\gamma_2^2)}$, where $\gamma_i = E_i/m_i$ for each hemisphere of the event). The missing momentum should be isolated, as quantified by $E_{\rm w}^{30}$ (see Fig. 1b). A veto on a high energy lepton reduces the WW background when one of the W's decays to e(μ)ν and an upper cut on the missing mass reduces the WW background when one of the W's decays to $\tau\nu$. To further reduce this background, a tau jet is searched for using the JADE algorithm with a y_{cut} of 0.001. The W mass (M_W) is computed as the mass of the hadronic system excluding the tau jet and α_{23} is defined as the smallest angle between the tau jet and the other jets. In the 4J-H and 4J-L analyses, the remaining $q\bar{q}$ radiative return background is reduced by vetoing events with an isolated photon with energy greater than 10 GeV. A photon is isolated if no particle is detected in a cone of 30° half angle around its direction, excluding an inner cone of 5° half angle. The cuts for the 4J-VH, 4J-H and 4J-L selections are listed in Table 2.

Two Jets and Lepton Topology (2JL) The characteristic signature of the 2JL channel is the presence of an energetic isolated lepton (see Fig. 1c). Here, lepton refers to e or μ, where electrons are identified using ECAL information. Cuts on the missing mass and the hadronic mass, $W_{\rm had}$, (the mass of the event, excluding the most energetic identified lepton) and $E_{\rm w}^{30}$ reduce the $q\bar{q}$ and WW backgrounds. The 2JL-L selection is sensitive to the $\tau^+\tau^-$ and $\gamma\gamma \to \tau^+\tau^-$ backgrounds, which are reduced by means of the hadronic mass and the acoplanarity. The cuts are listed in Table 2.

Very Low ΔM Selections The selections for the very low mass difference chargino signal are designed to reject the $\gamma\gamma$ background, mostly $\gamma\gamma \to$ *hadrons* and $\gamma\gamma \to \tau^+\tau^-$. In both 4J and 2JL selections, variables similar to those used for the other chargino analyses are employed, such as the missing transverse momentum, the transverse imbalance and the transverse acoplanarity. No energy should be detected at low angle. In the spirit of Section 3.2, energy-based variables are

Chargino - 4J		
ΔM range	VH,H	L
$M_{\rm vis}$	> 4 GeV/c^2 and trigger conditions	
$N_{\rm ch}$	≥ 7	≥ 4
$P_T \geq f_1\sqrt{s}$ / $f_2\sqrt{s}^{\dagger}$	$f_1 = 5\%,\ f_2 = 7.5\%$	
$\Delta\phi_{\rm T}$	$< 175°$	
E_{12}	$< 5\%\sqrt{s}$	$= 0$
$\theta_{\rm scat} > \theta_1$ or $\theta_{\rm point} > \theta_2$	$\theta_1 = 15°, \theta_2 = 5°$	$\theta_1 = 15°, \theta_2 = 10°$
$\lvert\cos\theta_{\rm miss}\rvert$	< 0.95	
F_{NH}	$< 45\%$	
$F_{NH} < f_1$ or $P_T^{\overline{NH}} > f_2$	$f_1 = 30\%, f_2 = 3\%\sqrt{s}$	
E_ℓ	$< 20\%\sqrt{s}$	
Thrust	< 0.9	
$E_{\rm w}^{30}$		$< 1.5\%\sqrt{s}$

Chargino - 2JL			
ΔM range	VH	H	L
$M_{\rm vis}$	> 4 GeV/c^2 and trigger conditions		
$N_{\rm ch}$	≥ 3		
identified e/μ	≥ 1		
$P_T \geq f_1\sqrt{s}$ / $f_2\sqrt{s}^{\dagger}$	$f_1 = 5\%,\ f_2 = 7.5\%$		$f_1 = 2.5\%,\ f_2 = 2.5\%$
$\Delta\phi_{\rm T}$	$< 175°$		
E_{12}	$< 5\%\sqrt{s}$		$= 0$
$\theta_{\rm scat} > \theta_1$ or $\theta_{\rm point} > \theta_2$	$\theta_1 = 15°, \theta_2 = 5°$		
$\lvert\cos\theta_{\rm miss}\rvert$			< 0.95
F_{NH}	$< 45\%$		
$min(E_{\rm w}^{30}, E_\ell^{30})$			$< 1\%\sqrt{s}$
E_ℓ	$< 30\%\sqrt{s}$	$< 20\%\sqrt{s}$	
$M_{\rm miss}$	$> 25\%\sqrt{s}$		

Neutralino - AJ		
ΔM range	H	L
$M_{\rm vis}$	> 4 GeV/c^2 and trigger conditions	
$N_{\rm ch}$	≥ 7	≥ 4
$P_T \geq f_1\sqrt{s}$ / $f_2\sqrt{s}^{\dagger}$	$f_1 = 5\%,\ f_2 = 7.5\%$	$f_1 = 3\%,\ f_2 = 4.5\%$
$P_T/E_{\rm vis}$	$> 20\%$	$> 40\%$
$\Delta\phi_{\rm T}$	$< 170°$	$< 120°$
$\Delta\phi$	$< 170°$	
E_{12}	$< 5\%\sqrt{s}$	$= 0$
$\theta_{\rm scat} > \theta_1$ or $\theta_{\rm point} > \theta_2$	$\theta_1 = 15°, \theta_2 = 5°$	
$\lvert\cos\theta_{\rm miss}\rvert$	< 0.95	
F_{NH}	$< 45\%$	
$F_{NH} < f_1$ or $P_T^{\overline{NH}} > f_2$	$f_1 = 30\%$	
	$f_2 = 3\%\sqrt{s}$	$f_2 = 1.8\%\sqrt{s}$
E_ℓ	$< 20\%\sqrt{s}$	
$E_{\rm w}^{30}$	$< 7.5\%\sqrt{s}$	$= 0$
$E_{30°}/E_{\rm vis}$	$< 70\%$	

Table 1: *Selection cuts against* $\gamma\gamma \to$ *hadrons. The* † *indicates that the cut is applied when the azimuthal angle of the missing momentum is within* 15° *of the vertical plane.*

complemented by direction-based variables such as $|\cos\theta_{\rm miss}|$, $\theta_{\rm scat}$ and $\theta_{\rm point}$. Events with fake neutral hadrons are removed with F_{NH} and $P_T^{\overline{NH}}$, as can be seen in Table 2. As the main potential background in the 2JL-VL selection comes from events with a misidentified hadron, cuts to identify leptons are tighter than in the other 2JL analyses and also use the d$E/$dx information from the TPC to identify signal electrons which typically have lower momentum than those targeted by the L, H, and VH selections. The momentum is required to be in excess of 1 GeV/c for electrons and 2.5 GeV/c for muons. The estimated $\gamma\gamma \to$ *hadrons* contamination is $\simeq$ 60 fb in 4J-VL and negligible in 2JL-VL.

Acoplanar Leptons Topology (AL) The acoplanar lepton selection is similar to the ALEPH selectron and smuon selections [2], with the exception that no lepton identification is required and events with four tracks are accepted, where three tracks are hypothesized as arising from a tau decay if their invariant mass is lower than 1.5 GeV/c^2. The cuts against WW background, specifically the requirement on the energy of the tracks ($E_{\ell 1}$ and $E_{\ell 2}$, where $E_{\ell 2} < E_{\ell 1}$), are optimised for the two chargino decay scenarios leading to an acoplanar lepton signature: $\chi^\pm \to \chi\ell\nu$ (three-body decay: AL-3) and $\chi^\pm \to \tilde{\nu}\ell$ (two-body decay: AL-2). Typical cut values for $\sqrt{s} = 172$ GeV are $E_{\ell 1} < 30$ GeV and $E_{\ell 2} < 26$ GeV for the AL-3 selection. Similar values of these cuts are applied in the AL-2 selection when $M_{\chi^\pm} - M_{\tilde{\nu}} < 20$ GeV/c^2.

For two body decays, the irreducible background from W pair production is subtracted. The optimisation of the upper cut on the energy of the leptons in the two-body decay selection takes this into account, and the cut applied depends on the mass difference between the chargino and sneutrino. The selection for small mass differences described in Ref. [2] is also applied in the analysis of the $\chi^\pm \to \tilde{\nu}\ell$ topology (AL-VL), requiring a pair of identified leptons, not necessarily of the same flavor. This analysis is also applied to the data taken at $\sqrt{s} = 130$ and 136 GeV, giving similar efficiencies and background as at $\sqrt{s} = 161$ and 172 GeV.

The background level and typical efficiency for each of the selections described above are listed in Table 4. To optimally search for a given chargino signal, some of the selections are combined as described in Section 3.5.

3.4 Neutralino selections

The neutralino analysis is optimised according to the various production and decay topologies in the different regions of the MSSM parameter space. The neutralino topologies can be summarised as follows. In the Higgsino region the only accessible channel is $\chi\chi'$ production and the signature consists of acoplanar jets. In the mixed region, heavier neutralinos (χ'', χ''') are also produced and give rise to cascade decays. For large slepton masses (large m_0) the final states are mainly multi-hadronic. For light slepton masses (small m_0) the leptonic branching ratios are enhanced, which gives rise to events containing several leptons in the final state. Furthermore, there are parameter configurations (in the mixed region for low $\tan\beta$, when the $\chi\chi'$ mass difference is small) for which the branching ratio for $\chi' \to \chi\gamma$ is large; therefore the events often contain isolated photons.

In other regions, neutralino decays to a neutral Higgs boson (h) may play a role, depending on the assumptions made for the Higgs sector. The efficiency for $\chi^j \to \chi h$ is greater than the efficiency

Chargino - 4J				
ΔM range	VH - 161 GeV	VH - 172 GeV	H	L
anti-$\gamma\gamma$ cuts	Yes			
$N_{\rm ch}$	≥ 24	≥ 26		
P_T	> 15 GeV/c	> 10 GeV/c		
$P_T/E_{\rm vis}$	$> 12.5\%$	$> 10\%$		
$M_{\rm vis}$	< 160 GeV/c^2		< 70 GeV/c^2	< 60 GeV/c^2
$\Delta\phi$	$< 165°$	$< 175°$		
$Inv\mathcal{B}$	> 0.4		> 0.3	> 0.25
$E_{\rm w}^{30}$	$< 10\%\sqrt{s}$		$< 8\%\sqrt{s}$	
E_ℓ	< 10 GeV	< 15 GeV		< 20 GeV
$M_{\rm miss}$	< 60 GeV/c^2	< 70 GeV/c^2		> 100 GeV/c^2
$M_W > M_1$ or $\alpha_{23} > \alpha_{\rm ref}$	$M_1 = 90$ GeV/c^2			
	$\alpha_{\rm ref} = 140°$	$\alpha_{\rm ref} = 80°$		
Thrust			< 0.85	< 0.925
Isolated γ			=0	

Chargino - 2JL				
ΔM range	VH - 161 GeV	VH - 172 GeV	H	L
anti-$\gamma\gamma$ cuts	Yes			
$N_{\rm ch}$	≥ 7			
E_ℓ	> 12.5 GeV	$\in [10, 40]$ GeV	$> 2.5\%\sqrt{s}$	< 20 GeV
$E_\ell^{30} < E_\ell^{\rm ref}$ and $E_{\rm w}^{30} < E_{\rm w}^{\rm ref}$ $(E_\ell^{\rm ref}, E_{\rm w}^{\rm ref}) \Rightarrow$	Yes $(5\%, 20\%)\sqrt{s}$	Yes $(2.5\%, 20\%)\sqrt{s}$	if $E_\ell^{30} > 0$ $(20\%, 4\%)\sqrt{s}$	No
$M_{\rm miss}$	> 50 GeV/c^2	> 55 GeV/c^2	> 50 GeV/c^2	> 120 GeV/c^2
$W_{\rm had}$	< 70 GeV/c^2	< 65 GeV/c^2	$\in [5, 45]$ GeV/c^2	> 1.5 GeV/c^2
Thrust				< 0.95
$\Delta\phi_{\rm T}$				$< 170°$ ($< 150°$ if $N_{\rm ch} \leq 4$)
Isolated γ			$= 0$	

Chargino - VL		
Topology	4J	2JL
$M_{\rm vis}$	> 4 GeV/c^2 and trigger conditions	
$M_{\rm miss}$	> 140 GeV/c^2	
$E_{\rm w}^{30}, E_{12}$	$= 0$ GeV	
$\theta_{\rm point}$	$> 10°$	
$\lvert\cos\theta_{\rm miss}\rvert$	< 0.8	
$N_{\rm ch}$	≥ 4	≥ 3
P_T	$> max(2.5\%\sqrt{s}, 40\%E_{\rm vis})$	$> 25\%E_{\rm vis}$
$\Delta\phi_{\rm T}$	$< 125°$	$< 160°$,$< 150°$ if $N_{\rm ch} = 4$ $< 110°$ if $N_{\rm ch} = 3$ and $\lvert\cos\theta_{\rm miss}\rvert > 0.7$
Thrust	< 0.95	0.9
F_{NH}	$= 0$ or $\overline{P_T^{NH}} > 2\%\sqrt{s}$	< 0.4
identified e/μ		≥ 1
E_ℓ^{30}		< 5 GeV
$\theta_{\rm scat}$		$> 2°$ if $P_T^{lepton} < 2$ GeV/c
$W_{\rm had}$		< 10 GeV/c^2

Table 2: *Cut values for the chargino analyses. The VH selections are divided into cuts used at* $\sqrt{s}=$ *161 GeV and 172 GeV. Cuts against* $\gamma\gamma \rightarrow$ *hadrons are listed in Table 1 for the L, H, and VH selections; all cuts for the VL selections are listed here.*

for $\chi^j \to \chi Z^*$, in part due to the $\nu\overline{\nu}$ decays of the Z^*. Conservatively, the branching ratios of decays to Higgs bosons are set to zero.

Four different analyses are used to cope with the various decay modes throughout the parameter space. The efficiencies and expected background levels for these analyses are summarised in Table 4.

Acoplanar Jets Topology (AJ) Two analyses are employed for this topology: the AJ-H analysis, optimised for large mass differences between χ and χ', and the AJ-L analysis, optimised to complement the AJ-H analysis for small mass differences ($\Delta M < 30$ GeV/c^2). In both cases, the dominant backgrounds after the cuts against the $\gamma\gamma$ background (see Table 1) are WW, $Z\gamma^*$ and Weν production. These backgrounds are rejected by placing a cut on the event thrust and on the visible mass (see Fig. 1d). The optimum cut on the visible mass can be parametrised with the simple form $M_{\text{vis}} < \Delta M + 5$ GeV/c^2 throughout the full Higgsino region. As the AJ-H selection is applied to regions of the parameter space with large mass differences, the visible mass cut is less effective to reduce the background and cuts on the event acoplanarity are introduced. All selections are summarised in Table 3.

Four Jets with Photons (4J-γ) In the mixed region, χ'' and χ''' can be produced with large cross sections. For large slepton masses, the cascade decays give rise to multi-hadronic final states similar to 4J chargino events. The 4J-H chargino analysis is used, with a visible mass cut re-optimised for the neutralino search.

In this region, the radiative decay of the χ' can be large, especially when the mass difference between the χ' and the χ is small, giving rise to hadronic final states with an isolated photon. A dedicated analysis has been designed for this topology: starting from the anti-$\gamma\gamma$ cuts of the 4J-H chargino analysis, an energetic isolated photon is required. To suppress the $Z\gamma^*$ and $q\overline{q}\gamma$ backgrounds, the acoplanarity should be smaller than 160° and the missing momentum isolated ($E_{\text{w}}^{30} < 7.5\%\sqrt{s}$). A variable cut on the visible mass is also imposed depending on the signal configuration. The background is about 36 fb (20 fb) at 172 GeV (161 GeV) for any cut on the visible mass, and is reduced to less than 5 fb when the visible mass is required to be smaller than 70 GeV. For example, when $\chi'\chi''$ production dominates and with a branching ratio for $\chi' \to \chi\gamma$ of 60%, the efficiency of both the 4J-γ analysis and the 4J-H analysis is about 15%, giving a total efficiency of 30% with about 40 fb of background at $\sqrt{s} = 172$ GeV. The cuts are summarised in Table 3.

Acoplanar Leptons Topology (AL-χ) When sleptons are light, the production of $\chi\chi'$ or $\chi\chi''$ pairs followed by the decay $\chi' \to \ell^+\ell^-\chi$, $\chi'' \to \ell^+\ell^-\chi$ has a sizeable rate and leads to final states containing two acoplanar leptons with the same flavour and missing energy. This topology resembles the production of slepton pairs, therefore similar selections to those described in Ref. [2] are used, except that the cuts against the (dominant) WW background are optimised for the neutralino searches as a function of the mass difference between the produced neutralinos. The WW background is reduced by requiring that the two leptons in the final state be of the same flavour, and by placing a cut on the maximum momentum of both leptons.

Neutralino			
Topology	AJ - H	AJ - L	4J-γ
anti-$\gamma\gamma$ cuts	Yes	Yes	Yes (4J-H)
$M_{\text{vis}}^{\dagger}$	< 45 GeV/c^2	< 35 GeV/c^2	< 70 GeV/c^2
Thrust	< 0.95		
$\Delta\phi$	$< 170°$		$< 160°$
$\Delta\phi_{\text{T}}$	$< 170°$		
E_{w}^{30}			$< 7.5\%\sqrt{s}$
isolated γ			1

Topology	ML
anti-$\gamma\gamma$ cuts	Yes (subset of 4J-H)
identified e/μ	$\geq$2e or $\geq 2\mu$
$E_{\ell 1}{}^{\dagger}$	$\in [5, 50]$ GeV
$E_{\ell 2}{}^{\dagger}$	> 5 GeV, $\in [5, 25]$ GeV if $E_\gamma < 10$ GeV
$M_{\text{vis}}^{\dagger}$	< 60 GeV/c^2

Table 3: *Cuts for neutralino analyses; cuts against $\gamma\gamma$ are listed in Table 1. The positions of the cuts for variables with a † depend on the point in the SUSY parameter space; typical values are given for illustration ($\Delta M = 40$ GeV/c^2 for AJ-H, $\Delta M = 30$ GeV/c^2 for AJ-L, $\tan\beta = \sqrt{2}$, $M_2 = 50$ GeV/c^2, $\mu = -68$ GeV/c^2, $m_0 = 75$ GeV/c^2 and $\sqrt{s} = 172$ GeV for ML).*

Multileptons Topology (ML) This analysis is used to cover the region of the parameter space where sleptons are light and where also the heaviest neutralinos are produced (for instance, the region with $m_0 = 75$ GeV/c^2, $M_2 < 130$ GeV/c^2, $\tan\beta = \sqrt{2}$). In this case, several leptons can be present in the final state. For example, the production of $\chi'\chi''$ pairs, followed by the decays $\chi' \to \ell^+\ell^-\chi$, $\chi'' \to \chi^\pm \ell\nu$, gives rise to at least three charged leptons in the event. The following selections are designed to select these topologies with high efficiency. Cuts against the two-photon background similar to those discussed for 4J-H in Section 3.2 are applied, but the cut on the minimum number of charged tracks, the thrust and on the maximum energy of the leading lepton are removed. Instead, at least two muons or two electrons are required (after removal of photon conversions). The leptons are ordered in energy, where $E_{\ell 1} > E_{\ell 2}$. The energies of the two leading leptons are required to be larger than 5 GeV. Cuts on the maximum energy of these leptons and on the maximum visible energy in the final state are also applied to reject WW and other backgrounds. These cuts are optimised as a function of the masses of the neutralinos. If an isolated photon with $E > 10$ GeV is present in the final state, as one would expect from the decay $\chi' \to \chi\gamma$, then the cut on the maximum energy of the second lepton is removed; this cut is directed against WW events which usually do not contain isolated photons. The ML selection is summarised in Table 3.

3.5 Combination of Selections

The many different selections developed for the chargino and neutralino searches must be combined so that the analysis is sensitive to all possible topologies for a large range of ΔM and decay branching ratios, without allowing excessive background from selections that contribute little to the efficiency for a particular signal configuration. The selections are combined according to the $\bar{N}_{95}$

Topology	$\sigma_{\rm bg}(161)$	$\sigma_{\rm bg}(172)$	ϵ	signal($M_{\chi^\pm}$,$M_{\chi,\tilde{\nu}}$)
Chargino - 4J				
VH	21 fb	34 fb	22%	(85,5)
H	29 fb	37 fb	54%	(85,40)
L	4 fb	15 fb	33%	(85,75)
VL	66 fb	65 fb	19%	(85,80)
Chargino - 2JL				
VH	25 fb	20 fb	35%	(85,5)
H	4 fb	2 fb	61%	(85,40)
L	9 fb	3 fb	47%	(85,75)
VL	9 fb	13 fb	21%	(85,80)
Chargino - AL				
AL-3	74 fb	88 fb	66%	(85,45)
AL-2	$45-119$ fb	$45-232$ fb	65%	(80,60)
AL-VL	80 fb	80 fb	19%	(80,76)
Neutralino				
AJ-H	22 fb	18 fb	38%	
AJ-L	35 fb	42 fb	24%	
4J-γ	5 fb	5 fb	15%	
ML	52 fb	51 fb	10%	
AL-χ	67 fb	56 fb	10%	

Table 4: *Efficiencies at* $\sqrt{s} = 172$ *GeV and background for chargino and neutralino analyses. The chargino efficiencies are determined considering only the topology for which that selection was optimised, for* $\mu = -500$ GeV/c^2 *and* $\tan\beta = \sqrt{2}$, *varying* M_1 *independently of* M_2 *to obtain the various* ($M_{\chi^\pm}, M_\chi$) *listed combinations. For the 2JL analyses, efficiencies are calculated for events with* $\ell = e, \mu$. *For the AL-2 analysis, the minimum and maximum background is given. The background for the neutralino selections is determined at the points given in Tables 3.*

prescription, by summing the signal efficiency and background expectations. The global analysis employs the combination of selections which, for a given choice of the relevant parameters, minimises the average expected limit on the production cross section. Although there are discontinuities in the efficiency, the average expected limit is continuous.

3.5.1 Combination of chargino selections

In the chargino analysis the relevant parameters are the chargino mass, ΔM, and the leptonic branching ratio. "Cross-efficiency" between selections is not negligible as some selections are sensitive to a topology other than that for which they were optimised; for example, the 4J selections are efficient for the 2JL topology when the lepton is a tau. There is also some overlap among the selections in the expected background.

For the typical case in the chargino analysis where the dominant decay is through a virtual W, only 10% of the signal events will have the topology of acoplanar leptons, while 44% will have a 2JL topology, and 46% will occur in the 4J topology. The selection for acoplanar leptons (AL-3) has irreducible background from W pair production, and so the average expected limit is not optimal when the acoplanar leptons selection is included.

When the branching ratio of $\chi^{\pm} \to l\nu\chi$ is greater than 60%, assuming equal branching ratios to e, μ, and τ leptons, a better limit is expected when the AL-3 selection is applied with the 4J-L, 2JL-H and 2JL-L selections. If stau mixing is allowed, an increase in the number of decays with τ leptons will be observed. The hadronic tau decays are more efficiently selected by the 4J selections, so a higher branching ratio to leptons is required before the AL-3 selection is included. Two-body decays, $\chi^{\pm} \to \tilde{\tau}_1\nu$, can also occur when stau mixing is considered, and the same combination of selections is applied for the resulting topology.

For two-body decays to sneutrinos, $\chi^{\pm} \to \ell\tilde{\nu}$, the AL-2 and AL-VL selections are applied to optimise the expected limit as a function of ΔM ($M_{\chi^{\pm}} - M_{\tilde{\nu}}$) and $M_{\chi^{\pm}}$; the AL-VL selection is applied when $\Delta M < 8$ GeV/c^2, for all $M_{\chi^{\pm}}$.

The optimisation for charginos is performed with the integrated luminosity at 172 GeV, finding the optimal combination of selections for a chargino with mass of 85 GeV/c^2, as the chargino limit is determined by that data set in most cases. The optimal combinations of selections for the 161 GeV data are then found for an 80 GeV/c^2 chargino by taking the expected 172 GeV results into account. Consequently, not all selections are used in the analysis of the 161 GeV data.

The combinations of selections applied to the data in the chargino analysis and the expected background estimates are summarised in Table 5.

3.5.2 Combination of neutralino selections

In the neutralino analysis the optimal combination depends on the region of the MSSM parameter space since the production processes and decay modes vary throughout this space.

In the Higgsino region the dominant topology is acoplanar jets, irrespective of m_0 and $\tan\beta$, and a combination of the AJ-H and AJ-L analyses is used for $\Delta M < 30$ GeV/c^2. For $\Delta M > 30$ GeV/c^2 the AJ-H analysis alone is used.

Charginos			
172 GeV			
	ΔM (GeV/c^2)	Combinations	σ_{bg} (fb)
1	< 10	4J-VL, 2JL-VL, 2JL-L	81
2	$10 - 50$	4J-L, 2JL-L, 4J-H, 2JL-H	53
3	≥ 50	4J-H, 2JL-H, 4J-VH, 2JL-VH	94
4	all	4J-L, 2JL-L, 2JL-H, AL-3	101
161 GeV			
	ΔM (GeV/c^2)	Combinations	σ_{bg} (fb)
1	< 10	2JL-VL, 4J-L, 2JL-L	23
2	$10 - 60$	4J-L, 4J-H, 2JL-H	34
3	≥ 60	2JL-H, 4J-VH, 2JL-VH	49
4	all	4J-L, 2JL-H, AL-3	90

Table 5: *Combinations of selections used to set limits with the 161 and 172 GeV data, for three-body decays of charginos. For combinations listed in Rows 1-3,* W^* *branching ratios are assumed, and the combinations in Row 4 are applied when the branching ratio of* $\chi^{\pm} \rightarrow \ell\nu\chi$ *is greater than* 60%. *Background estimations for the combinations are also given.*

Neutralinos						
			172 GeV		161 GeV	
	Region	Combinations	ϵ (%)	σ_{bg} (fb)	ϵ (%)	σ_{bg} (fb)
1	Higgsino:$\Delta M < 30$ GeV/c^2	AJ-L, AJ-H	39	46	40	41
2	Higgsino:$\Delta M > 30$ GeV/c^2	AJ-H	38	18	41	22
3	mixed:high Br($\chi' \rightarrow \chi\gamma$)	4J-H, 4J-γ	30	38	30	30
4	mixed:low m_0	AJ-H, ML, AL-χ	23	108	23	95

Table 6: *Combinations of selections used to set limits with the 161 and 172 GeV data, for the neutralino searches. The parameters for efficiency and background measurements are the same as in Table 3.*

In the mixed region, χ'' and χ''' production is kinematically accessible and, in addition, the χ' has a large radiative branching fraction when $\mu < 0$. Thus for large slepton masses ($m_0 \sim 200$ GeV/c^2), where the neutralinos give rise mainly to hadronic final states, a combination of the 4J-H chargino analysis with the 4J-γ analysis gives the best sensitivity. For small slepton masses ($m_0 = 75$ GeV/c^2, for example), the leptonic branching ratios are enhanced and the AJ-H analysis is combined with the AL-χ and ML analyses over the mixed and gaugino regions. Since in these regions the neutralino production processes and the leptonic and hadronic branching ratios change rapidly as a function of the parameters, the combination of the AJ-H, AL-χ and ML selections allows for a robust analysis and for a stable signal efficiency.

The combinations of selections, efficiencies, and background measurements for the neutralino searches are summarised in Table 6.

3.6 Efficiency Parametrisation

The efficiency of the chargino selections at its simplest level is governed by the visible mass of the event. This is highly correlated with ΔM, which, when sleptons are heavy, is equivalent to the maximum invariant mass Q^2 of the fermion pair from the decay of the virtual W. However, the field content of the charginos and neutralinos can affect the selection efficiency independently of $M_{\chi^\pm}$ and M_χ. The gaugino and Higgsino components for both the $\chi^\pm$ and χ play a role in the decay amplitude. The CP eigenvalues (embedded in the neutralino mass matrix) can influence the differential decay rate $d\Gamma/dQ^2$ [9]. Aside from discrete differences in CP eigenvalues, the $\widetilde{\mathrm{W}}^+$ and $\widetilde{\mathrm{H}}^+$ components in the decay amplitude depend on the model parameters in different ways, showing up as significant changes in $d\Gamma/dQ^2$, even for constant $M_{\chi^\pm}, M_\chi$ and dominantly gaugino-like charginos and neutralinos. These effects have the largest impact on the efficiency when $\Delta M \approx 50$ GeV/c^2, and can lead to differences in the efficiency of up to 30% (relative) in some cases.

For the selections described here, the efficiencies are derived separately for $\tan\beta = \sqrt{2}$ and 35. The efficiencies are $\sim 5\%$ lower for the latter, when $\Delta M \sim 40 - 50$ GeV. These differences are verified with both DFGT and SUSYGEN.

To map out the dependence of the efficiency as a function of ΔM, μ is fixed to a large value, and $\tan\beta$ is fixed to $\sqrt{2}$ and 35. After finding M_2 for a given $M_{\chi^\pm}$, M_1 is varied (thereby violating the standard gaugino mass unification relation) to obtain the full range of M_χ (hence, ΔM). Many points in ΔM are generated using the full detector simulation, with a statistical error of $\sim 1\%$ for each ΔM point.

The efficiencies are parametrised as functions of ΔM in the three ranges of ΔM given in Table 5. They are also parametrised for the three chargino decay topologies: “QQ”, when both charginos decay to $q\bar{q}'\chi$, “QL”, when one chargino decays to $\ell\nu\chi$ ($\ell = e, \mu, \tau$) and the other to $q\bar{q}'\chi$, and “LL”, when both charginos decay to $\ell\nu\chi$. This is done to allow for variations of the leptonic branching ratio, $\mathrm{Br}(\chi^\pm \to \ell\nu\chi)$.

Separate parametrisations are obtained for $\sqrt{s} = 161$ and 172 GeV. A corrective factor (one for each ΔM range) is derived for the $M_{\chi^\pm}$ dependence at fixed $\sqrt{s}$. Corrections are applied for increases in the relative fraction of chargino decays to taus in proportion to all leptons. Corrections are also applied for the systematic reduction in efficiency as discussed in Section 3.7.

The efficiencies as a function of ΔM and $\mathrm{Br}(\chi^\pm \to \ell\nu\chi)$ for the chargino analysis are shown in Fig. 2. The efficiency is shown as a function of ΔM for the combinations in rows $1 - 3$ of Table 5. Efficiencies are shown separately for the “QQ” and “QL” signal topologies. The efficiency for the “LL” topology is essentially zero for these combinations of selections. The efficiencies for the different topologies are combined according to the appropriate branching ratios to give an overall efficiency; here, W branching ratios are applied. Also shown is the efficiency as a function of $\mathrm{Br}(\chi^\pm \to \ell\nu\chi)$ under the assumption of equal branching ratios to e, μ and τ, and assuming 100% branching ratio to $\tau\nu\chi$, which gives the most conservative efficiency if stau mixing is allowed. The sudden increase in the efficiency at large $\mathrm{Br}(\chi^\pm \to \ell\nu\chi)$ is due to the effect of including the AL-3 selection.

The selection efficiencies for AJ and two-body chargino decays ($\chi^\pm \to \ell\tilde{\nu}$ and $\chi^\pm \to \tilde{\tau}_1\nu$) are parametrised similarly. The efficiency for the AJ analysis is shown in Fig. 3 as a function of ΔM for different values of the MSSM parameters (m_0, $\tan\beta$, μ) and for $\sqrt{s} = 161$ GeV. For this analysis, in the Higgsino region, the efficiency depends only on the mass difference between the two neutralinos, *i.e.,* on the visible energy in the final state, and not on other parameters of the theory. In this region, independent of the other model parameters, the only kinematically accessible process is $\chi\chi'$ production and the dominant decay of the χ' is $\chi' \rightarrow \mathrm{Z}^{*}\chi$. The efficiency improves at large ΔM due to the larger visible energy in the final state, and drops at $\Delta M = 30$ GeV/c^2 because of the change in the combination of selections.

3.7 Studies of Systematic Effects

The most important systematic effects for the chargino and neutralino analyses are those which affect the signal efficiency, including modelling of the signal process and detector.

The requirement that no energy be reconstructed within 12° of the beam axis introduces an inefficiency due to beam-associated and detector background not simulated by Monte Carlo, as it depends on the beam conditions during data taking. This loss is measured from events triggered at random beam crossings to be 4.1% in the 161 GeV data and 2.4% in the 172 GeV data. The efficiency for the relevant selections is reduced accordingly.

To check the simulation of the detector response to events which are kinematically similar to the signal events, a sample of events from LEP 1 is selected. These events have an isolated energetic photon from final state radiation, which is removed from the analysis of the rest of the event, leaving an acoplanar hadronic system with missing energy and visible mass similar to signal events. Kinematic quantities such as thrust, transverse momentum, acoplanarity, isolation of the missing momentum vector, and the neutral hadronic energy fraction are well reproduced by the Monte Carlo. The simulation of kinematic quantities for low visible mass systems is tested by comparison to $\mathrm{Z} \rightarrow \tau^{+}\tau^{-}$ events, and good agreement is found.

The identification of electrons and muons has been compared in data and Monte Carlo. The electron identification efficiency for the 2JL-VH, H, and L has a systematic uncertainty of 0.6% per electron. The selection for the 2JL-VL analysis has a systematic uncertainty associated with the electron identification efficiency at low momenta due to the simulation of the calorimetric and $\mathrm{d}E/\mathrm{d}x$ estimators of 3.7%, with an additional correction of −3.9% (relative) applied to the efficiency. Systematic uncertainties in the muon identification lead to an error of 0.7% in the 2JL-VH, H, and L selections, 1.4% in the 2JL-VL selection.

The Monte Carlo program used for simulating the chargino signal, DFGT, has been compared to SUSYGEN, and good agreement found for kinematic variables and signal efficiencies predicted by the two programs. The effects of the spin of the charginos is evident in the angular distribution of the leptons; however, this has an insignificant effect on the overall efficiency. The DFGT program does not include a simulation of final state radiation. The effect of this on the selection efficiency varies from $\simeq 1\%$ for high ΔM to 3.5% for very low ΔM. Signal efficiency measurements are corrected for this effect.

The measurement of the luminosity and beam energy can introduce an error in the derivation of an upper limit on the signal. The uncertainty on the measurement of the integrated luminosity recorded by the detector is less than 1% including statistical and systematic uncertainties. The beam energy is known to within 30 MeV [24], causing a negligible uncertainty in the results of this analysis.

Systematic errors are taken into account in the derivation of the results for the chargino and neutralino analyses by means of the method detailed in [25]. In addition to the systematic uncertainties, statistical errors from the Monte Carlo statistics and the luminosity measurement, which have uncertainties of $\lesssim 1\%$ each are taken into account.

4 Results

4.1 Events selected in the data

In the 21 pb^{-1} data taken at $\sqrt{s} = 161 - 172$ GeV, 9.5 events are expected from background in the chargino selections and 5.7 in the neutralino selections. There is some overlap in the background expectations for the chargino and neutralino analyses, leading to a total of 13 events expected. A total of 15 events is observed in the data, with some events selected by both the chargino and neutralino analyses, and several events selected by other ALEPH searches for supersymmetry [2, 3]. A summary of the events selected by each analysis, along with a Standard Model hypothesis for each candidate, is given in Table 7. The numbers of events expected and observed by the various combinations of selections is given in Table 8.

In the chargino analysis, a total of 3.7 events are expected to be selected by the 4J and 2JL analyses in the 161 and 172 GeV data set, and five events are observed. Two events are selected by the 4J-VL analysis in the 172 GeV data set; both are consistent with $\gamma\gamma$ background. One of these events has missing momentum pointing to the vertical LCAL crack; an undetected electron from a tagged $\gamma\gamma$ event is a possible explanation. The other event has an energy deposit in the HCAL which, possibly due to incorrect reconstruction, is not associated to a track, giving the event "extra" transverse momentum. Two events are selected by the 2JL-VH and 4J-VH selections, one each in the 161 and 172 GeV data; both are compatible with WW production. One event can be interpreted as WW $\rightarrow \tau\nu q\overline{q}$, where the tau decays hadronically. Due to a nuclear interaction in the ITC/TPC wall, the kinematics of the event are mismeasured. The other event can also be interpreted as WW $\rightarrow \tau\nu q\overline{q}$, where the tau decays to an electron and neutrinos. A possible mismeasurement of the energy of a low-angle jet due to cracks in the detector allows this event to be selected. The kinematics of the event selected by the 4J-L analysis in the 161 GeV data suggest its origin as the four-fermion process $\mathrm{ZZ}^*/\gamma^* \rightarrow \nu\overline{\nu}\tau^+\tau^-$ where the taus decay to ρ and a_1. This event is also selected by the searches for neutralinos, stops, and staus.

In the AL-3 selection, three events are observed in the 172 GeV data, while 1.6 are expected in the entire data set. One of these events is also selected by the smuon search, and is compatible with WW or $\mathrm{Z}\gamma^*$ production. The other two events are consistent with WW $\rightarrow \tau\nu\tau\nu$, with one-prong tau decays. The events are not selected by the slepton searches because the tracks are not both identified as leptons. In the AL-2 selection, the same three events are selected by the high mass difference analysis, while 3.8 events are expected from the 161 and 172 GeV data set. Five events, compatible with background processes, are selected by the AL-VL analysis, while two are expected, as described in Ref. [2].

In the neutralino analyses, two events are selected by the AJ-L and AJ-H analyses, while 1.9 are expected. Both events are among those selected by the chargino analysis. One event is observed in the data by the combination of the 4J-H and the 4J-γ analyses, while 0.8 are expected. This candidate is selected by the 4J-H analysis only for the neutralino case, where the optimisation

	Selection		
$\sqrt{s}$ (GeV)	Chargino	Neutralino	Hypothesis
161	4J-VH		WW
	AL-VL		$\gamma\gamma \to \ell\ell$
		AL-χ,ML	WW, Zγ^*
	4J-L	AJ-L	ZZ$^*/\gamma^* \to \tau\tau$
172	2JL-VH		WW
	AL-VL		$\gamma\gamma \to \ell\ell$
	AL-3,AL-2	ML	WW, Zγ^*
		4J-H	WW
	4J-VL		$\gamma\gamma \to q\bar{q}$
	AL-VL		$\gamma\gamma \to \ell\ell$
	AL-3,AL-2		WW
	AL-3,AL-2		WW
	4J-VL	AJ-L	$\gamma\gamma \to \tau\tau$
	AL-VL		$\gamma\gamma \to \ell\ell$
	AL-VL		$\gamma\gamma \to \ell\ell$

Table 7: *Candidate events selected by the chargino and neutralino analyses in the 161 and 172 GeV data.*

Chargino			Neutralino		
Combination	N$_{exp}$	N$_{obs}$	Combination	N$_{exp}$	N$_{obs}$
1	1.1	3	Higgsino: $1-2$	1.9	2
W^* 2	0.9	1	mixed: 3	0.8	1
3	1.5	2	mixed: 4	3.0	2
$\chi^{\pm}(\ell)$	5.8	8			
total	9.5	13	total	5.7	5

Table 8: *Numbers of background events expected and observed by the chargino and neutralino analyses in the 161 and 172 GeV data. In the chargino column, the "W^*" combinations correspond to rows $1-3$ of Table 5, and the neutralino combinations correspond to those given in Table 6. "$\chi^{\pm}(\ell)$" refers to the total number of events from AL-3,AL-2, and AL-VL selections (see Table 4).*

procedure leads to a visible mass cut above 70 GeV/c^2, in contrast to the chargino search. This event has a visible mass of 70.3 GeV/c^2 and shows a large charged track multiplicity. There is a clear sign of an isolated minimum ionising particle at low angle, with a muon-like digital pattern in the HCAL and one hit in each muon chamber layer. No charged track is reconstructed because the particle is at a very low angle: only two TPC hits are recorded. This favours the WW interpretation of this event, with a leptonic decay of one W.

Finally, two events are selected while three are expected in the combination of the AJ-H, AL and ML analyses optimised for the neutralino search for small m_0 in the mixed region. One of them is common to the chargino candidate sample. The other one is a slepton candidate and is described in detail in Ref. [2].

The number of events selected in the data, their distribution among the selections and their properties do not suggest a signal for supersymmetry. Therefore, limits are set on the production of charginos and neutralinos, and constraints placed on the parameters of the MSSM. The candidate events are taken into account in deriving the limits in the regions of $(M_{\chi^\pm}, M_\chi)$ and $(M_{\chi'}, M_\chi)$ in which the analyses that select each candidate are applied. For the combinations using the AL-2 selection only, the WW background is subtracted [26] from the AL-2 selection.

4.2 Limits on the production cross section

Upper limits on sparticle production cross sections can be derived from the results of these searches. Unless sleptons are light, W^* exchange dominates the decay of charginos, so the process $\mathrm{e}^+\mathrm{e}^- \to \chi^+\chi^- \to \mathrm{W}^*\chi\mathrm{W}^*\chi$ defines the signal topology used to set upper limits on the cross section in the plane of $M_{\chi^\pm}$ and M_χ, shown in Fig. 4. The efficiencies used in the derivation of this limit are calculated for $\mu = -500\ \mathrm{GeV}/c^2, \tan\beta = \sqrt{2}$, using the techniques described in Section 3.6. The features of the contours of constant cross section reflect discontinuities in the number of candidates at points where the combinations of selections change and where the additional luminosity from data taken at lower energies applies. The integrated luminosities taken at centre-of-mass energies of 130, 136 [27], 161, and 170 GeV are scaled by the ratio of cross sections in the gaugino region ($\mu = -500\ \mathrm{GeV}/c^2, \tan\beta = \sqrt{2}$) to those at 172 GeV, and included with the data taken at 172 GeV to derive this limit. The ratio of cross sections is slightly larger in the gaugino region than in the Higgsino region; however, the result differs by less than 10%.

Similarly, the neutralino AJ-H and AJ-L searches can be used to derive an upper limit on the cross section for $\chi\chi'$ production, where the decay $\chi' \to \mathrm{Z}^*\chi$ is assumed. The resulting cross section limit for the range of $(M_{\chi'}, M_\chi)$ relevant in the Higgsino region is shown in Fig. 5. Values of $\Delta M > 40\ \mathrm{GeV}/c^2$ have not been considered because for the given luminosity, the cross sections are too low to allow this region to be useful as a constraint.

4.3 Interpretation in the MSSM

The constraints that the results of the chargino and neutralino searches can place on the parameters of the MSSM are explored in this section. First, limits are derived assuming that sleptons are heavy. In this case, charginos and neutralinos decay with W and Z branching ratios, respectively. Next, sleptons are allowed to be light, and the resulting changes to the cross section and decay branching ratios are explored. Stau mixing can potentially affect the limits derived from the searches, as the decays of charginos and neutralinos are modified by the presence of a light stau. These effects have been investigated, and the resulting limits are only slightly modified from previous cases. Assumptions commonly made in SUSY GUT's are then relaxed, and exclusion limits independent of requirements of a universal slepton mass are derived. The assumption of a universal gaugino mass is also relaxed, and finally, limits without assumptions on a universal scalar or a universal gaugino mass are given.

Limits are derived using parametrisations for the efficiencies, as described in Section 3.6, and the slight variations in efficiency due to field content are checked with the full MSSM simulation.

4.3.1 Standard scenario: heavy sleptons

Chargino and neutralino masses and cross sections are determined by the parameters μ and M_2, for given values of $\tan\beta$ and m_0. Limits on the production of charginos and neutralinos constrain these parameters, as depicted in Fig. 6 for the given values of $\tan\beta$ and for $M_{\tilde{\nu}} = 200$ GeV/c^2. At this value of $M_{\tilde{\nu}}$, the decay branching ratios are unaffected, but the cross section is reduced with respect to its asymptotic value. (When sleptons are heavy, detailed assumptions made on the relations among their masses are unimportant.)

In the gaugino region, the chargino production cross section is high, and selection efficiency is high since $\Delta M \simeq M_{\chi^\pm}/2$ (see Fig. 2). As a result, charginos are excluded nearly to the kinematic limit. The limit on the chargino mass is 85.5 GeV/c^2 for $\mu = -500$ GeV/c^2 and $\tan\beta = \sqrt{2}$. In the Higgsino region, the cross section is lower and ΔM is small, leading to a lower selection efficiency due to the difficulties of rejecting $\gamma\gamma$ background, and a slightly weaker limit ($M_{\chi^\pm} > 85$ GeV/c^2 for $\Delta M > 10$ GeV/c^2, corresponding to $M_2 \lesssim 550$ GeV/c^2). The additional gain from the search for $\chi\chi'$ production, which is most powerful in the Higgsino and mixed regions for low $\tan\beta$, is also shown. For high $\tan\beta$, the result from the chargino searches is similar, and the exclusion reaches the kinematic limit; no additional exclusion is gained from the neutralino search. In the following, the discussion will be concentrated on the low $\tan\beta$ case.

The impact of the neutralino search is seen more clearly in Fig. 7. The limit on the chargino mass as a function of M_2 is derived using the chargino and neutralino analyses separately. For lower M_2, charginos are excluded nearly to the kinematic limit by the chargino search alone. The neutralino analysis allows exclusion beyond the kinematic limit for chargino production. For higher M_2, ΔM becomes small, leading to a lower selection efficiency. The abrupt reduction in the limit from the chargino search at $M_2 \sim 550$ GeV/c^2 is due to the increase in the number of candidates to be taken into account for $\Delta M < 10$ GeV/c^2.

Charginos and neutralinos constitute independent signals in the Higgsino region. The selection criteria developed for the chargino signal do not augment significantly the neutralino acceptance, and vice versa. To obtain a combined limit, expected signals and numbers of candidates are summed, extending the exclusion in the Higgsino region, as shown in Fig. 7. This is most evident in the deep Higgsino region, where the combination of chargino and neutralino analyses sets a limit on the chargino mass above 79 GeV/c^2 , for $M_2 \leq 1200$ GeV/c^2 (corresponding to $\Delta M \geq 5$ GeV/c^2). This improves the limit of 72 GeV/c^2 set by the chargino search alone.

At the "Supersymmetric Limit", where $\tan\beta = 1$ and $M_2 = \mu = 0$, both $\chi^\pm$ and $\chi_2^\pm$ have mass $\simeq M_{\mathrm{W}}$. The two lightest neutralinos are nearly massless, and χ' decays to $\chi\gamma$ with 100% branching ratio. Production of heavier neutralinos is also kinematically possible, with $M_{\chi''} \simeq M_{\chi'''} \simeq M_{\mathrm{Z}}$. This process was accessible at $\sqrt{s} = 130 - 136$ GeV, and was used to exclude the Supersymmetric Limit [28]. At $\sqrt{s} > 2M_{\mathrm{W}}$, direct exclusion of this region using chargino searches also is possible. Since the mass difference between the charginos and neutralinos is $\simeq 80$ GeV/c^2, the search is difficult due to the WW background, but the efficiency of the 2JL-VH and 4J-VH selections allows this point to be excluded. The optimal limit is expected when only the data taken at $\sqrt{s} = 172$ GeV is included. No background is subtracted in the derivation of this limit. The upper limit on the cross section is 2.9 pb, and at $\sqrt{s} = 172$ GeV, the theoretical cross section is > 2.9 pb in this region. This limit is derived for $m_0 = 200$ GeV/c^2.

4.3.2 Effects of light sleptons

The effect of low slepton masses is significant in both the production and decay of charginos and neutralinos, as explained in Section 1. Here limits are derived from the chargino and neutralino searches when sleptons are light and the particular role played by staus is clarified. Direct searches for sleptons can also play a role in the chargino and neutralino limits in this scenario. A general exclusion will be treated fully in a forthcoming publication; for preliminary results, see Ref. [30].

Light sleptons, nominal stau mixing

The limit on the chargino mass throughout the gaugino region is evaluated as a function of μ for several values of m_0 and for $\tan\beta = \sqrt{2}$, as shown in Fig. 8a. This limit is derived from the chargino analysis assuming a universal scalar mass m_0 for the sleptons. The overall reduction in the limit for decreasing m_0 is due to the diminished cross section. As charginos become more gaugino-like (*i.e.,* as $|\mu|$ increases), the leptonic branching ratio increases, and the selection for acoplanar leptons is applied to retain efficiency; the sharp change in the limit is due to the change in efficiency and number of candidates. Stau mixing, discussed further below, is calculated with $A_\tau = 0$ GeV/c^2 (at the electroweak scale).

The evaluation of low m_0 effects is extended to the (μ, M_2) plane, as shown in Fig. 8b. The reduction of the limit in the gaugino region, as seen in the previous plot, is also evident in the mixed region, where a "valley" opens up for $-\mu \approx M_2$. There is a modest improvement in the excluded region from charginos as m_0 increases from 200 GeV/c^2 to 1000 GeV/c^2. In the Higgsino region, light scalars have little effect on the exclusion obtained with the chargino and neutralino searches, and all limits are similar to the high m_0 results.

In contrast to chargino production, the neutralino cross section increases significantly as m_0 is reduced below 100 GeV/c^2. The enhancement of the leptonic branching ratios motivates the combination of the acoplanar jet analysis with the multi-leptonic analyses. The results cover the chargino valley and slightly improve the LEP 1 limit [29] (not shown). In the gaugino region where only $\chi\chi'$ and $\chi'\chi'$ are produced, the larger cross section for $m_0 = 75$ GeV/c^2 allows the derivation of limits which are almost as constraining as the chargino limits. The limits from neutralino searches for $m_0 = 75$ GeV/c^2 are expressed as a limit on the chargino mass in Fig. 8a.

In chargino production and decay for low m_0, the relevant physical quantity is the mass of the sneutrino, as this determines the reduction in cross section and enhancement of the leptonic branching ratio. Therefore, the limit on the chargino mass can be meaningfully expressed as a function of the sneutrino mass.

As seen in Fig. 9 for two points in the gaugino region, when $M_{\tilde{\nu}} \geq 150$ GeV/c^2, there is little effect due to the sneutrino mass; this is similar to the case under which the limits in Fig. 6 are derived. The cross section decreases as $M_{\tilde{\nu}}$ decreases, and the leptonic branching ratio increases, necessitating a change in selections to include the AL-3 selection. In the near gaugino region ($\mu = -80$ GeV/c^2), light sleptons have less of an effect, and the leptonic branching ratio does not increase above 50%. The limit in this case is lower than for $\mu = -500$ GeV/c^2 due to the lower cross section.

When $M_{\tilde{\nu}} \leq M_{\chi^\pm}$, two-body decays $\chi^\pm \rightarrow \ell\tilde{\nu}$ tend to dominate. The AL-2 and AL-VL selections are used to derive the limit in this region. When the mass difference is too small, the leptons do not have enough energy to pass the selection, and no exclusion is obtained. This is the "corridor" visible at low $M_{\tilde{\nu}}$ in Fig. 9, which extends to the LEP 1 limit of 45 GeV/c^2 on the chargino mass. The differences in the corridor for these two values of μ are due to the effects of stau mixing, discussed in the following subsection. The features of the contour reflect the accounting for candidates as a function of ΔM. Also shown is the limit from the slepton search [2], which excludes the corridor where no limit can be obtained from the chargino search. The slepton limit is derived for $\tan\beta = \sqrt{2}$ and $\mu = -80$ GeV/c^2, and is much weaker for high $\tan\beta$; thus, a general exclusion of this region is difficult.

Effects of stau mixing

Due to the relatively high mass of the tau lepton, mixing between the left- and right-handed staus can occur, modulated by the off-diagonal term in the stau mass matrix, $-M_\tau(A_\tau + \mu\tan\beta)$. The lightest stau, $\tilde{\tau}_1$, can be significantly lighter than the other sleptons and sneutrinos, causing an increase in the branching ratios of charginos and neutralinos to final states with taus. The decay amplitude also depends on the field content of the chargino or neutralino, and is most enhanced in the gaugino region. Thus, the effects of stau mixing are most evident for gaugino-like charginos and neutralinos.

To study the effects of stau mixing, a point in the deep gaugino region is chosen, specifically $\mu = -500$ GeV/c^2, for $\tan\beta = \sqrt{2}$. A low value of $\tan\beta$ is chosen since for high $\tan\beta$ in the gaugino region, the stau mass can become unphysical ($M^2_{\tilde{\tau}_1} < 0$), for low m_0. The limit on the chargino mass as a function of sneutrino mass (still assuming a universal slepton mass) is shown in Fig. 10 for three values of the tri-linear coupling term, A_τ: $A_\tau = 0$ and $A_\tau = \pm 1$ TeV/c^2.

For high $M_{\tilde{\nu}}$, there is little effect from stau mixing, and the results are as discussed previously. As $M_{\tilde{\nu}}$ decreases, the slepton masses also decrease, with a comparatively larger impact of the mass splitting in the stau sector. However, even if the detailed behaviour of the chargino mass limit as a function of $M_{\tilde{\nu}}$ is affected by the precise value of A_τ, the global features observed for $A_\tau = 0$ remain. The differences shown in Fig. 10 are due to the mass of $\tilde{\tau}_1$ and its coupling to the chargino. Decays of $\chi^\pm \to \tilde{\tau}_1\nu$ can occur concurrently with $\chi^\pm \to \ell\tilde{\nu}$ or $\chi^\pm \to \ell\nu\chi$, with branching ratios which depend on the degree of mixing, causing changes in the details of the limit.

For $A_\tau = 0$, $\chi^\pm \to \tilde{\tau}_1\nu$ decays can occur when $\chi^\pm \to \ell\tilde{\nu}$ is kinematically forbidden, and the effects are only noticeable in the limit near the corridor. For $A_\tau = +1$ TeV/c^2, the $\tilde{\tau}_1$ is heavier than for $A_\tau = 0$, and there are few $\chi^\pm \to \tilde{\tau}_1\nu$ decays. A larger difference is observed for $A_\tau = -1$ TeV/c^2, as the $\tilde{\tau}_1$ is light and $\chi^\pm \to \tilde{\tau}_1\nu$ decays occur with a high branching ratio. This allows the corridor to be excluded but weakens the exclusion for lower $M_{\tilde{\nu}}$.

The effects of stau mixing depend on the mixing parameters and field content of the chargino. The most conservative limit is found by using the lowest efficiency. When the chargino decays to three-body final states, this is obtained when the highest possible branching ratio to final states with taus occurs, thereby maximising the impact of stau mixing. This is achieved by varying $M_{\tilde{\tau}_1}$ and the mixing angle to obtain the highest branching ratio for three-body decays to $\tau\nu\chi$ (without relying on constraints on A_τ). This limit is derived for $\mu = -500$ GeV/c^2, where a branching ratio of $\sim 85\%$ for $\chi^\pm \to \tau\nu\chi$ for all sneutrino masses is obtained, for $M_{\tilde{\nu}} > M_{\chi^\pm}$. Since the chargino selections have good sensitivity for final states with taus (see Fig. 2), the limit in this "maximal impact" case is not very different from the other examples. The result is shown as the hatched region in Fig. 10.

The limit on the chargino mass when the requirement of three-body decays is released is shown in Fig. 11, as a function of the $\widetilde{\tau}_1$ mass for a series of sneutrino masses. The transition from three-body ($\tau\nu\chi$) to two-body ($\widetilde{\tau}_1\nu$) final states is marked by the diagonal line; the bound falls by a small amount due to the increase of the final states with taus from $\sim 85\%$ to 100%. Allowing for $\chi^\pm \rightarrow \tilde{\tau}_1\nu$ decays degrades the limit by only a few GeV/c^2 as long as $M_{\widetilde{\tau}_1} - M_\chi \gtrsim 10$ GeV/c^2. As before, the mixing angle has been varied to obtain the lowest bound on the chargino mass. Generally this means that the $\widetilde{\tau}_1$ has a high left-stau component, leading to 100% $\chi^\pm \rightarrow \tilde{\tau}_1\nu$ decays. When $\chi^\pm \rightarrow \ell\tilde{\nu}$ decays are possible, the most conservative scenario is allowing $\chi^\pm \rightarrow \ell\tilde{\nu}$ decays to dominate, as this opens up the corridor discussed previously, and the limit on the chargino mass is $M_{\chi^\pm} = M_{\tilde{\nu}}$ (as shown in Fig. 11, for $M_{\tilde{\nu}} = 60$ GeV/c^2). This corresponds to requiring the $\widetilde{\tau}_1$ to have a maximal right-stau component. Limits from direct searches for staus can be invoked in that case, as shown in Fig 11 ("$\tilde{\tau}_{\mathrm{R}}$"). Also shown is the limit for staus which decouple from the Z ("$\tilde{\tau}_{\mathrm{min}}$"), which gives the most conservative limit from the stau search.

4.3.3 Non-universal scalar masses

Interpretation of search results often rely on assumptions according to a model. The assumption of a universal slepton mass at the GUT scale was made in the discussion of stau mixing effects for specific values of $A_\tau(0, \pm 1$ TeV/$c^2)$. However, in chargino decays, the sneutrinos and left sleptons are most relevant; the pure right sleptons do not play an important role. Therefore, theoretical constraints relating the masses of the left and right sleptons and sneutrinos can be dropped, retaining simply $M^2_{\tilde{\ell}L} = M^2_{\tilde{\nu}} - M^2_{\mathrm{W}} \cos 2\beta$, which is guaranteed by gauge invariance. Equal masses among slepton generations are assumed.

In this framework, the results previously derived from the chargino search are still valid apart from the stau mixing effects. The limit in the "maximal impact" case is valid without requiring assumptions on a universal scalar mass, as the most conservative limit is found independently of the mass of the right-stau. The requirement of three-body decays is retained for the "maximal impact" definition, for convenience in generalising the result. As shown in Fig. 11, there is little change in the limit when two-body decays are allowed.

4.3.4 Non-universal gaugino masses

If the unification relation between M_1 and M_2 is assumed, the mass difference between the chargino and lightest neutralino depends on the parameters of the MSSM: in the gaugino region, ΔM is $\simeq M_{\chi^\pm}/2$; for low negative μ and M_2, ΔM can be higher; in the Higgsino region ΔM becomes very small. Fig. 12a shows the limit on the chargino mass as a function of ΔM throughout the range of ΔM which can be attained in the gaugino and Higgsino region, for heavy sleptons ($M_{\tilde{\nu}} \geq 200$ GeV/c^2).

If the gauge unification condition is relaxed, the tight correspondence between the $\chi^\pm$ and χ masses in the gaugino region can be broken. Varying M_1 and M_2 independently, the limit on the chargino mass is displayed as a function of ΔM in Fig. 12a, for $\tan\beta = \sqrt{2}$. The two hatched bands show the spread in the limit as μ is varied between -500 and -80 GeV/c^2, with one band calculated assuming heavy sleptons and the other by maximising the impact of stau mixing (for three-body decays) as defined in Section 4.3.3. The plot shows the range $0.01 < \alpha < 10$ which is required to attain the entire range of ΔM, where α is defined by $\alpha = M_1/(\frac{5}{3}\tan^2\theta_W M_2)$. (This range of α is larger than is expected in typical SUSY GUT's.) The reach of the search into the region of very high ΔM is shown; for a nearly massless neutralino, the limit on the chargino mass is 82 GeV/c^2. These limits change little with $\tan\beta$, and are valid for high m_0 ($\geq$200 GeV/c^2).

An excluded region in the $(M_{\chi^\pm}, M_\chi)$ plane can be derived for a series of sneutrino masses, as shown in Fig. 12b. In addition to dropping gaugino mass unification, scalar mass unification is relaxed, and the maximum impact of stau mixing requiring three-body decays is taken into account.

5 Conclusion

The data recorded with the ALEPH detector at centre-of-mass energies of 161, 170, and 172 GeV have been examined for signals of chargino and neutralino production. Selections sensitive to topologies arising from chargino production were developed for a wide range of mass difference between the chargino and lightest neutralino, and especially for very high and very low ΔM. Additional selections were developed for topologies arising from chargino and heavier neutralino decays when sleptons are light. In all of the chargino analyses, 9.5 events were expected, and in the neutralino analyses, 5.7 events were expected, with some overlap between the background expectations, giving a total of 13 events expected. A total of 15 candidate events is observed in the data. These events are consistent with Standard Model processes, giving no evidence of a signal.

Limits at 95% C.L. on the production of charginos and neutralinos have been derived, and bounds placed on the parameters of the MSSM. The diversity of topological selections and wide range of sensitivity allow interpretation under a variety of model assumptions. Assuming unification of gaugino masses and that sleptons are heavy, limits are set on the chargino mass, for $\tan\beta = \sqrt{2}$. The limit is 85.5 GeV/c^2 in the gaugino region ($\mu = -500$ GeV/c^2), and 85.0 GeV/c^2 in the Higgsino region ($M_2 = 500$ GeV/c^2). The addition of the neutralino bounds allows the exclusion of charginos beyond the kinematic limit for chargino pair production, for moderate M_2 and low $\tan\beta$. The combination of chargino and neutralino searches extends the exclusion in the extreme Higgsino region, giving a lower limit on the chargino mass of 79 GeV/c^2 for $\Delta M \geq 5$ GeV/c^2 ($M_2 < 1200$ GeV/c^2), and $\tan\beta = \sqrt{2}$.

The search results have been interpreted also in the case of light sleptons. The neutralino search gives powerful exclusion limits in the mixed and gaugino region. The effect of stau mixing has been investigated in detail, and limits derived under various conditions. A limit has been obtained with few assumptions about the slepton sector by maximising the impact of stau mixing.

The gaugino mass unification condition has been relaxed, and limits derived for a wide range of ΔM, corresponding to extreme violations of the gaugino mass relation. In addition, scalar mass unification relations have been released, and limits derived for a range of sneutrino masses, which are independent of assumptions on the mass relations among sleptons and gauginos at the GUT scale, requiring only that $M_{\chi^\pm} < M_{\tilde{\nu}}, M_{\tilde{\tau}_1}$.

Acknowledgements

We thank and congratulate our colleagues in the accelerator divisions for the successful startup of LEP2. We gratefully acknowledge the support of the engineers and technicians in our home institutions. Those of us from non-member states thank CERN for its hospitality and support.

References

[1] H.P. Nilles, Phys. Rep. **110** (1984) 1;
H.E. Haber and G.L. Kane, Phys. Rep. **117** (1985) 76;
M. Chen, C. Dionisi, M. Martinez and X. Tata, Phys. Rep. **159** (1988) 201;
R. Barbieri, Riv. Nuovo Cim. **11** No. 4 (1988) 1.

[2] ALEPH Collaboration, CERN **PPE/97-056**, to be published in Phys. Lett. **B**.

[3] ALEPH Collaboration, CERN **PPE/97-084**, to be published in Phys. Lett. **B**.

[4] ALEPH Collaboration, CERN **PPE/97-071**, to be published in Phys. Lett. **B**.

[5] OPAL Collaboration, CERN **PPE/97-083**, submitted to Z. Phys. **C**.

[6] J. Ellis and F. Zwirner, Nucl. Phys. **B338** (1990) 317;
L. E. Ibanez and C. Lopez, *ibid.* **B233** (1984) 511;
K. Inoue, A. Kakuto, H. Komatsu and S. Takeshita, Prog. Theor. Phys. **68** (1982) 927;
ibid. **71**(1984) 413.

[7] CDF Collaboration, Phys. Rev. Lett. **74** (1995) 2626;
D0 Collaboration, Phys. Rev. Lett. **79** (1997) 1197;
D0 Collaboration, FERMILAB-PUB-97/172-E, hep-ex/9706014.

[8] W.A. Bardeen *et al.*, Phys. Lett. **B320** (1994) 110.

[9] A. Bartl, H. Fraas and W. Majerotto, Z. Phys. **C30** (1986) 441;
A. Bartl, H. Fraas and W. Majerotto, Z. Phys. **C41** (1988) 475;
A. Bartl, H. Fraas, W. Majerotto and B. Mösslacher, Z. Phys. **C55** (1992) 257.

[10] A. Bartl, H. Fraas and W. Majerotto, Nucl. Phys. **B278** (1986) 1;
S. Ambrosanio and B. Mele, Phys. Rev. **D52** (1995) 3900.

[11] D0 Collaboration, Phys. Rev. Lett. **75** (1995) 618;
CDF Collaboration, Phys. Rev. Lett. **76** (1996) 2006;
D0 Collaboration, Phys. Rev. Lett. **76** (1996) 2222;
CDF Collaboration, Phys. Rev. **D56** (1997) R1357.

[12] ALEPH Collaboration, Phys. Lett. **B384** (1996) 427.

[13] ALEPH Collaboration, Nucl. Inst. Meth. **A294** (1990) 121.

[14] ALEPH Collaboration, Nucl. Inst. Meth. **A360** (1995) 481.

[15] C. Dionisi, K. Fujii, S. Giagu and T. Tsukamoto, in *Physics at LEP2*, Eds: G. Altarelli, T. Sjöstrand, F. Zwirner, CERN Report 96–01, Volume 2 (1996) 337.

[16] T. Sjöstrand, Comp. Phys. Comm. **82** (1994) 74.

[17] S. Katsanevas and S. Melachroinos, in *Physics at LEP2*, Eds: G. Altarelli, T. Sjöstrand, F. Zwirner, CERN Report 96–01, Volume 2 (1996) 328.

[18] E. Barberio and Z. Was, Comp. Phys. Comm. **79** (1994) 291.

[19] S. Jadach and Z. Was, Comp. Phys. Comm. **36** (1985) 191.

[20] H. Anlauf *et al.*, Comp. Phys. Comm. **79** (1994) 466.

[21] M. Skrzypek, S. Jadach, W. Placzek and Z. Was, Comp. Phys. Comm. **94** (1996) 216.

[22] J.A.M. Vermaseren in *Proceedings of the IVth international Workshop on Gamma Gamma Interactions*, Eds G. Cochard, and P. Kessler, Springer Verlag, 1980;
ALEPH Collaboration, Phys. Lett. **B313** (1993) 509.

[23] T. Sjöstrand, Comp. Phys. Comm. **82** (1994) 74;
ibid., CERN-TH 7112/93 (1993, revised August 1994).

[24] LEP Energy Working Group, LEP Energy Group/97-01;
http://www.cern.ch/LEPECAL/reports/reports.html .

[25] R.D. Cousins and W.L. Highland, Nucl. Inst. Meth. **A320** (1992) 331-335.

[26] R.M. Barnett *et al.*, (Particle Data Group), Phys. Rev. **D54** (1996) 1.

[27] ALEPH Collaboration, Phys. Lett. **B373** (1996) 246.

[28] ALEPH Collaboration, Z. Phys. **C72** (1996) 549-559.

[29] OPAL Collaboration, Phys. Lett. **B377** (1996) 273.

[30] ALEPH Collaboration, "Update of the Mass Limit for the Lightest Neutralino", contribution to the International Europhysics Conference on High Energy Physics, Jerusalem, Israel, $19-26$ Aug. 1997, Ref. no. 594.

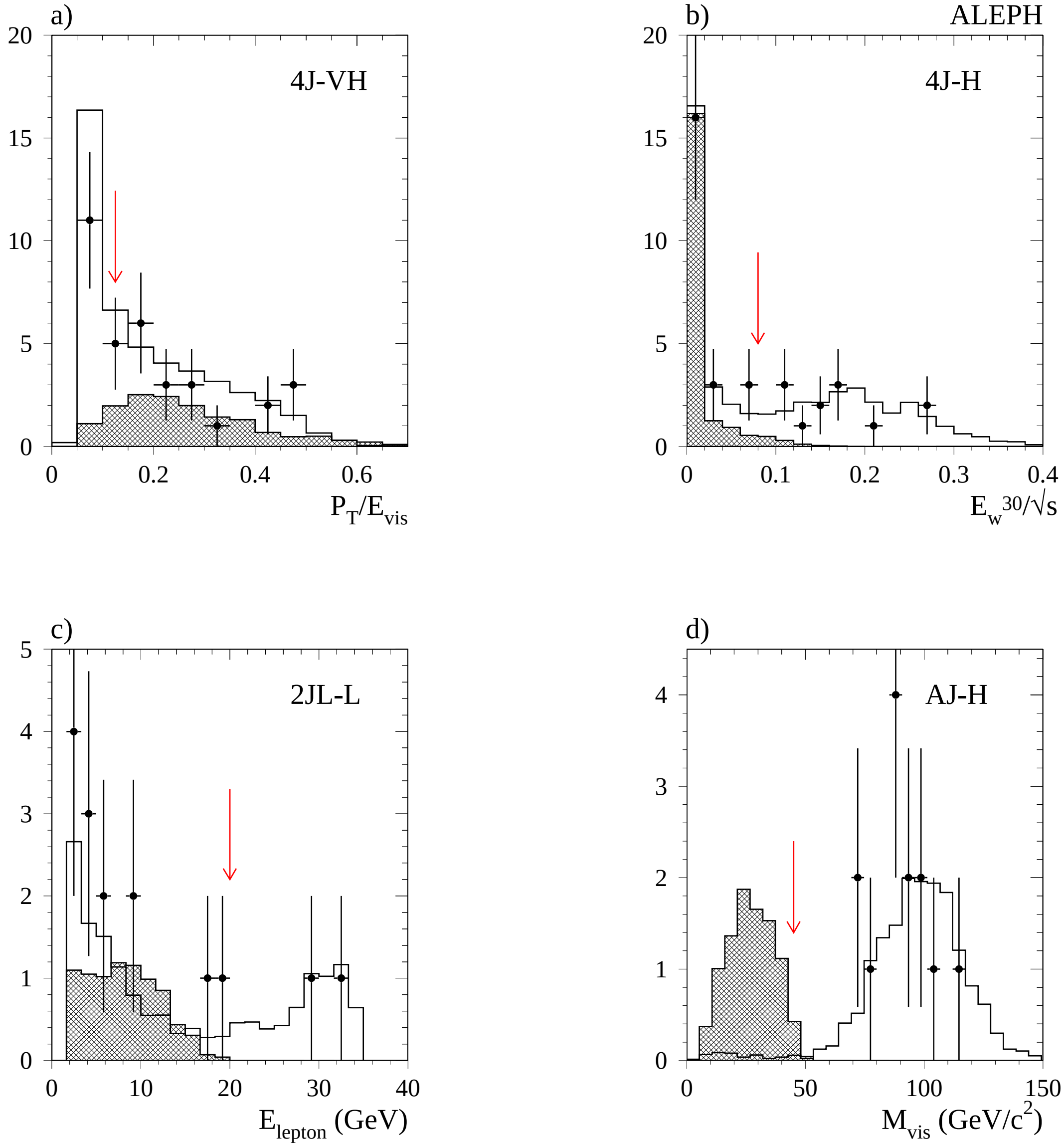

Figure 1: *Distributions after* $\gamma\gamma \to$ *hadrons rejection cuts, for* $\sqrt{s} = 172$ *GeV, of a)* P_T/E_{vis} *for the 4J-VH selection, b)* E_{w}^{30} *for the 4J-H selection, c)* E_ℓ *for the 2JL-L selection and d)* M_{vis} *for the AJ-H selection. Points with error bars represent the data; the solid histogram is the background Monte Carlo; the shaded histogram represents a signal configuration typical of each analysis* $(M_{\chi^\pm} - M_\chi(\text{GeV}/c^2))$ = *a) 85-05 b) 85-45 c) 85-65 and d)* $(M_{\chi'} - M_\chi)$ = *95-60. Background MC and signal are normalised to the integrated luminosity of the data. Signal cross-sections were determined for* $\tan\beta = \sqrt{2}$ *and for large slepton and sneutrino masses. The location of the cut is indicated with an arrow.*

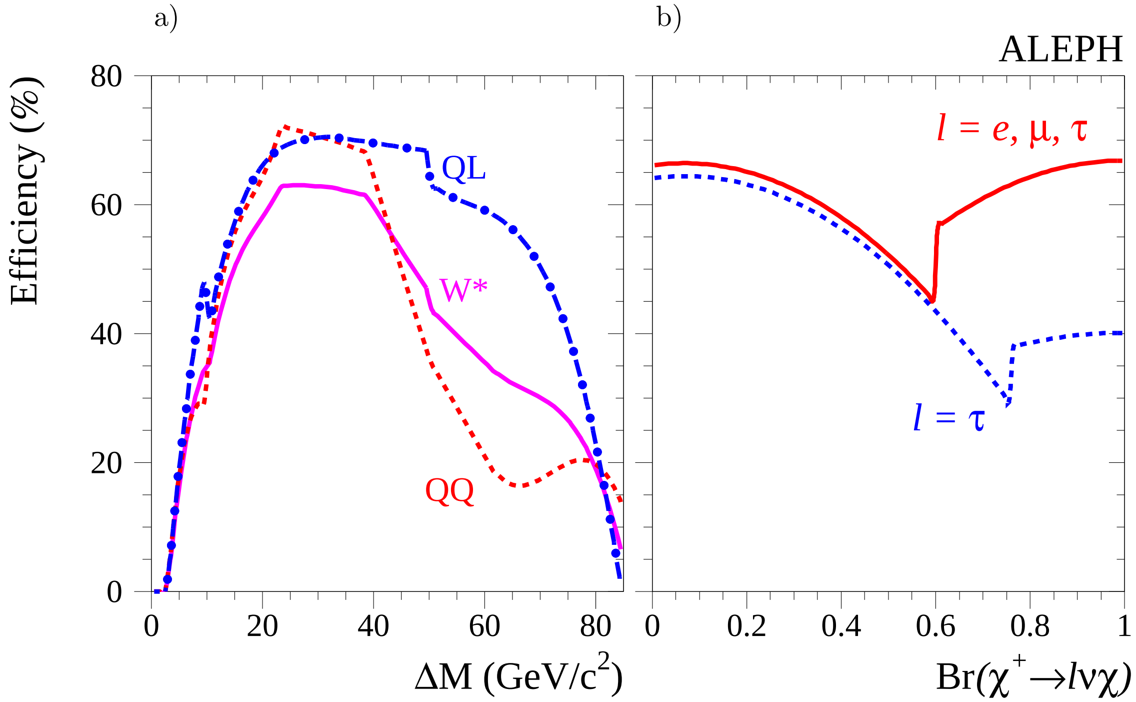

Figure 2: *Parametrised selection efficiency for the chargino selections listed in Table 5. a) The efficiency is plotted as a function of* ΔM*, for* $M_{\chi^{\pm}} = 85\ \mathrm{GeV}/c^2$ *at* $\sqrt{s} = 172$ *GeV, calculated for* $\mu = -500\ \mathrm{GeV}/c^2$ *and* $\tan\beta = \sqrt{2}$*, using the combinations for W branching ratios. Efficiencies are plotted for mixed ("QL") and hadronic ("QQ") topologies, and combined assuming W branching ratios,* $Br(\chi^{\pm} \to \ell\nu\chi) = 0.33$ *("W*"). b) The efficiency is plotted as a function of* $Br(\chi^{\pm} \to \ell\nu\chi)$*, assuming equal lepton flavours ("*$\ell = e, \mu, \tau$*") and that all leptons are taus ("*$\ell = \tau$*"), for* $\Delta M = 40\ \mathrm{GeV}/c^2$.

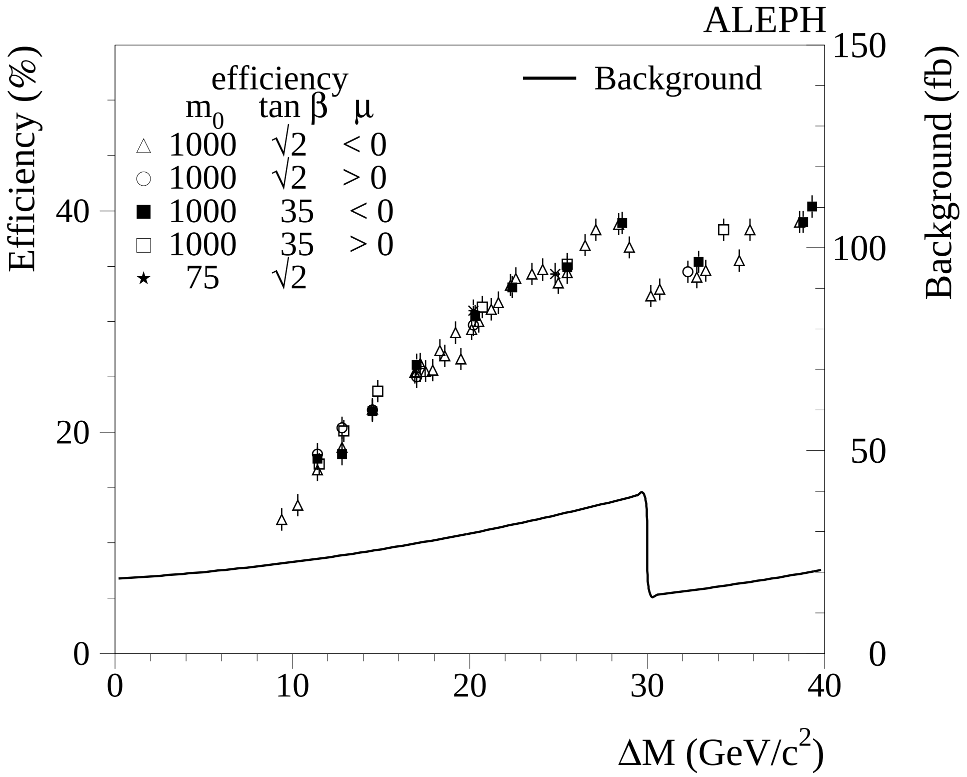

Figure 3: *The $\chi\chi'$ selection efficiency for AJ selections in the Higgsino region and expected background as a function of the mass difference between the two neutralinos, for $\sqrt{s} = 161$ GeV. Efficiencies are similar at $\sqrt{s} = 172$ GeV. The different symbols refer to different values of the model parameters.*

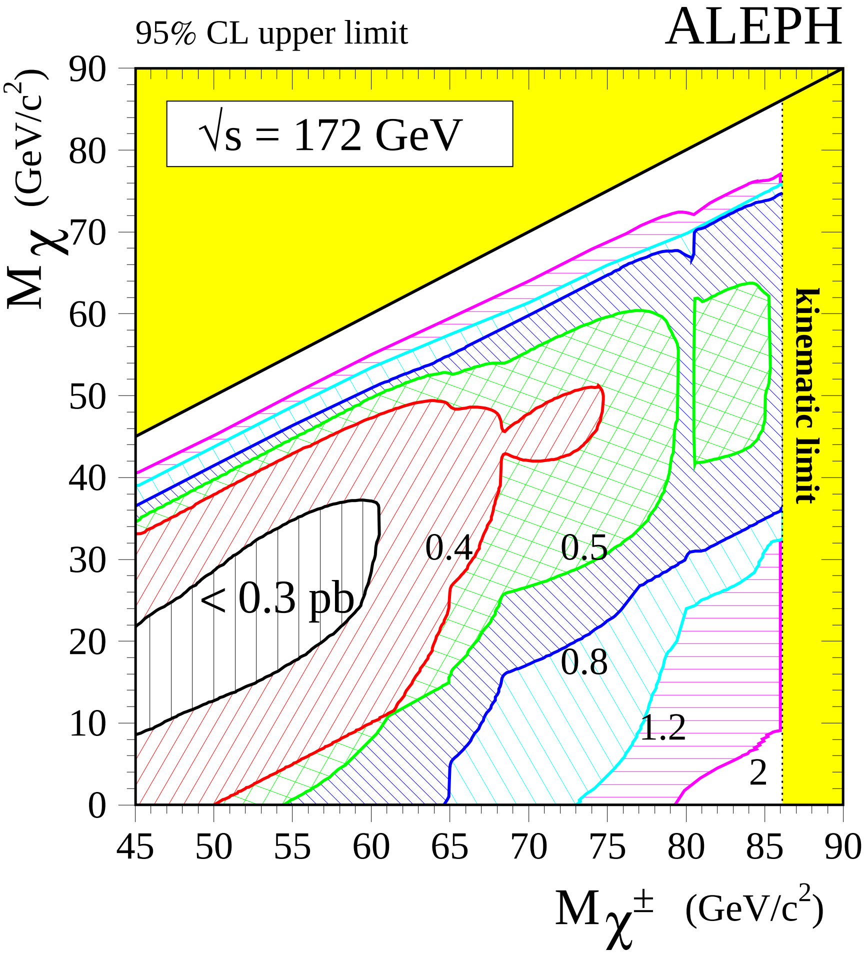

Figure 4: *The 95% C.L. upper limit on the cross section for chargino pair production, in the* $(M_{\chi^{\pm}}, M_{\chi})$ *plane. Data taken at lower centre-of-mass energies (130, 136, 161, and 170 GeV) are included by scaling the luminosity by the ratio of the cross section at that energy to the cross section at* $\sqrt{s} = 172$ *GeV , for* $\mu = -500$ GeV/c^2 *and* $\tan\beta = \sqrt{2}$. *W branching ratios are assumed in the chargino decay.*

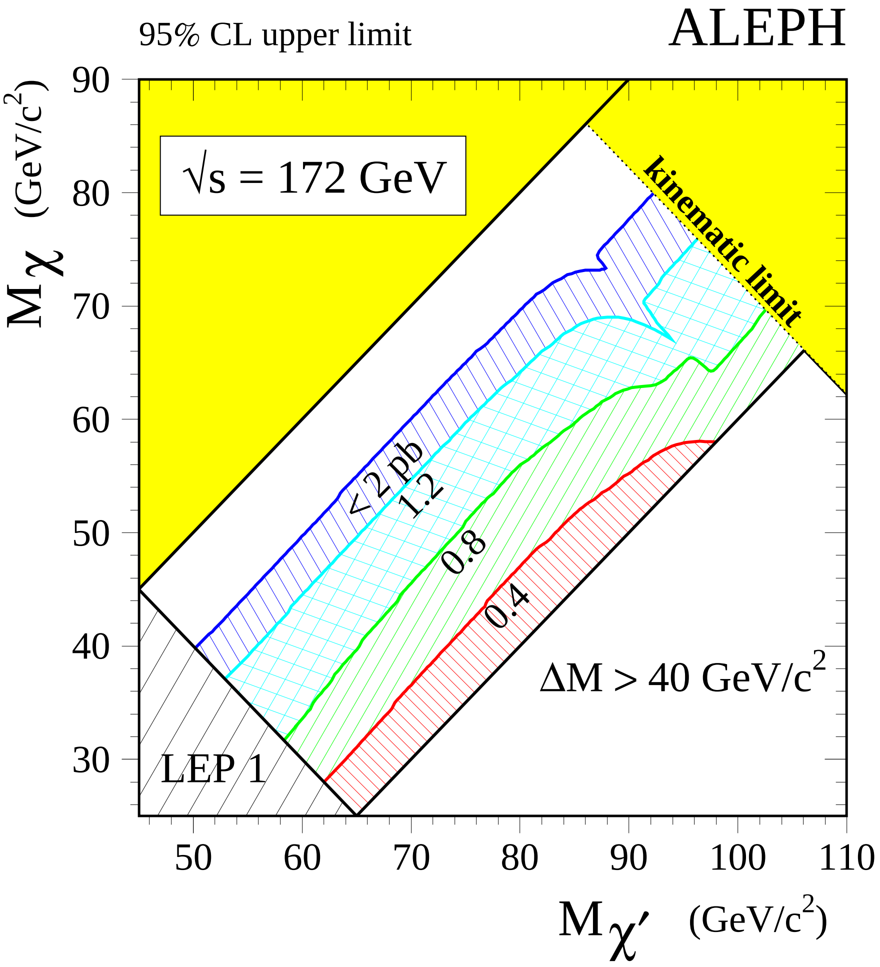

Figure 5: *The 95% C.L. upper limit on the cross section for* $\chi'\chi$ *production, in the* $(M_{\chi'}, M_{\chi})$ *plane, for the neutralino mass ranges relevant in the Higgsino region* ($\Delta M < 40$ GeV/c^2)*. The region where* $\Delta M > 40$ GeV/c^2 *has not been investigated. Data taken at lower centre-of-mass energies (130, 136, 161, and 170 GeV) are included by scaling the luminosity by the ratio of the cross section at that energy to the cross section at* $\sqrt{s}$=172 *GeV. Z branching ratios are assumed in the* χ' *decay.*

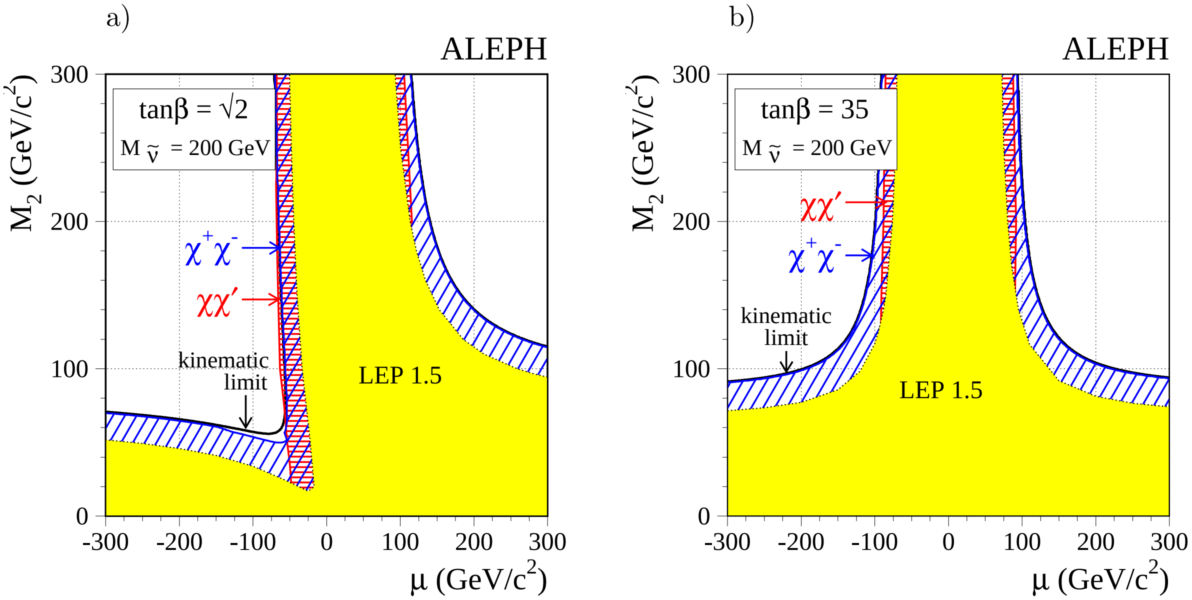

Figure 6: *Excluded region in the* (μ, M_2) *plane, for a)* $\tan\beta = \sqrt{2}$ *and b)* $\tan\beta = 35$, *and* $M_{\tilde{\nu}} = 200$ GeV/c^2. *The light grey region was obtained at LEP 1.5 [27]. The dark line shows the kinematic limit for chargino production at* $\sqrt{s} = 172.3$ *GeV. The slanted hatched region shows the region excluded by the chargino search, and the horizontal hatched region, by the neutralino search.*

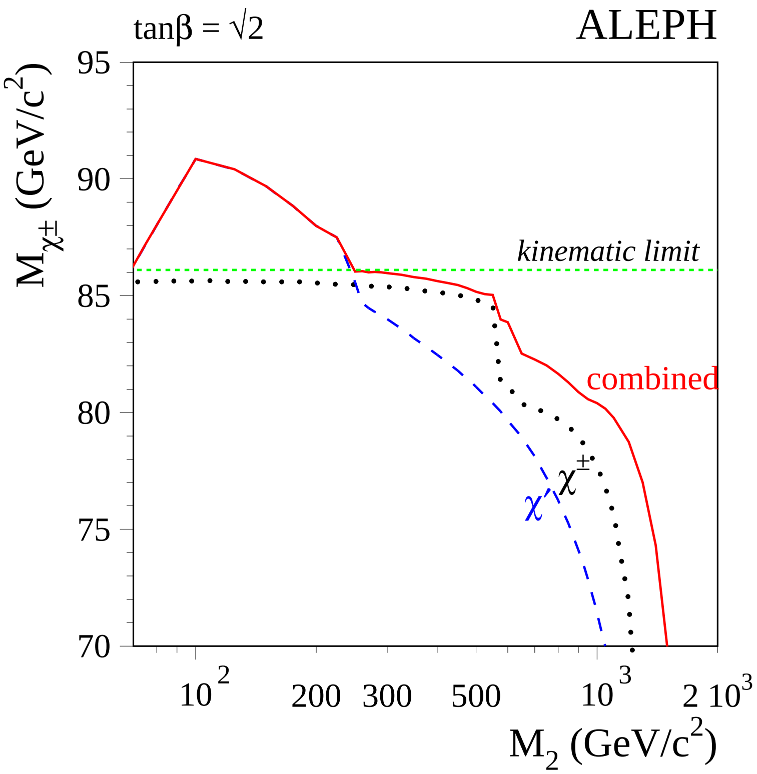

Figure 7: *The limit on the chargino mass as a function of* M_2*, from the chargino search (labelled* $\chi^{\pm}$*), from the neutralino search (labelled* χ'*), and from the combination of chargino and neutralino searches. This limit is derived for* $\tan\beta = \sqrt{2}$ *and* $m_0 = 200$ GeV/c^2.

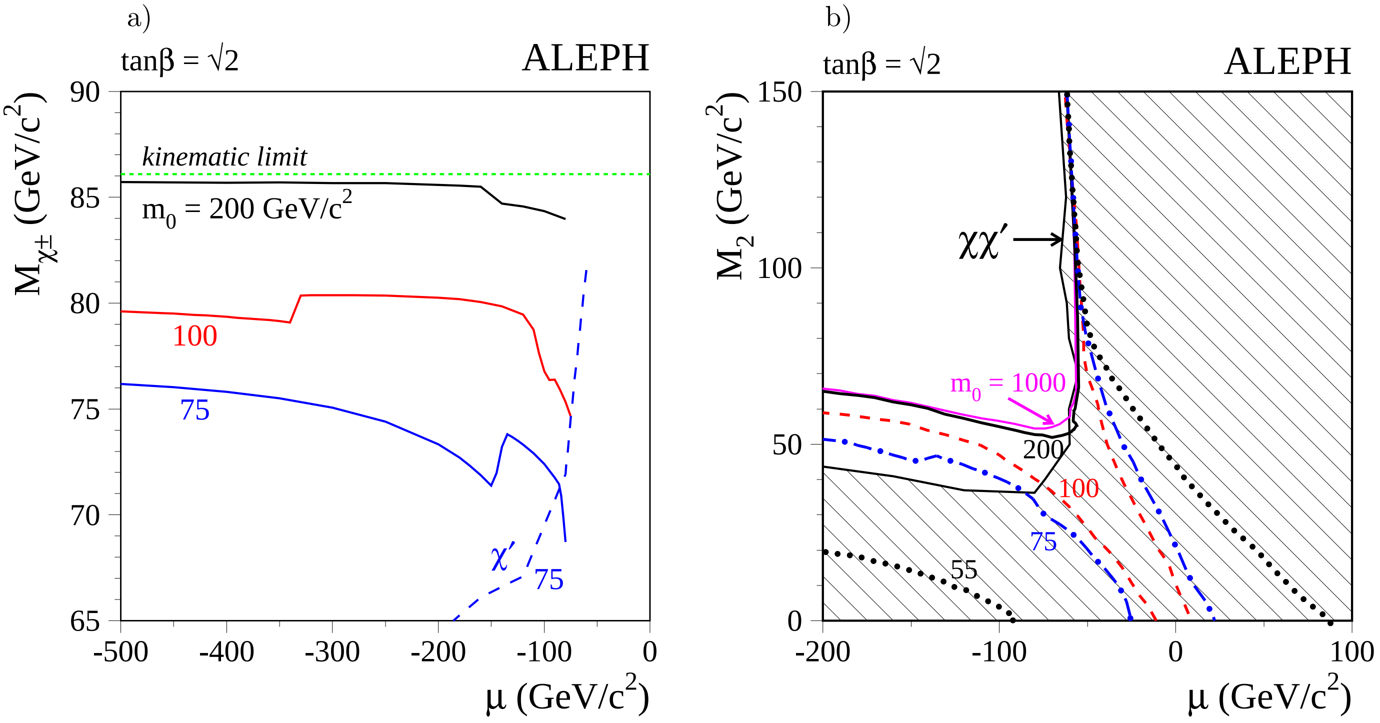

Figure 8: *a) The limit on the chargino mass as a function of* μ *for* $\tan\beta = \sqrt{2}$*, for several values of* m_0*. The excluded chargino mass from the neutralino search for* $m_0 = 75$ GeV/c^2 *is shown as a dashed curve. The chargino exclusion is independent of* μ *when* $\mu \gtrsim -60$ GeV/c^2*, as can be seen in b), where the exclusion in the* (μ, M_2) *plane for several values of* m_0 *is shown. The dark curves indicate limits from the chargino searches, and the hatched area is the exclusion from the neutralino analysis, for* $m_0 = 75$ GeV/c^2*. These limits are derived for* $\tan\beta = \sqrt{2}$*.*

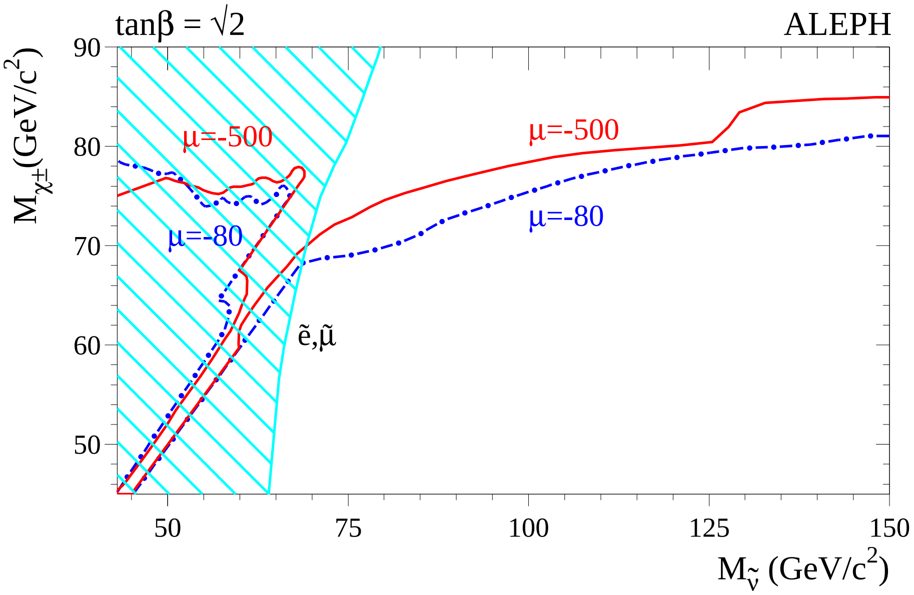

Figure 9: *The limit on the chargino mass as a function of sneutrino mass in the gaugino region, for* $\tan\beta = \sqrt{2}$ *and* $A_\tau = 0$*. The limit from selectron and smuon searches for* $\tan\beta = \sqrt{2}$ *and* $\mu = -80\ \mathrm{GeV}/c^2$ *is also indicated.*

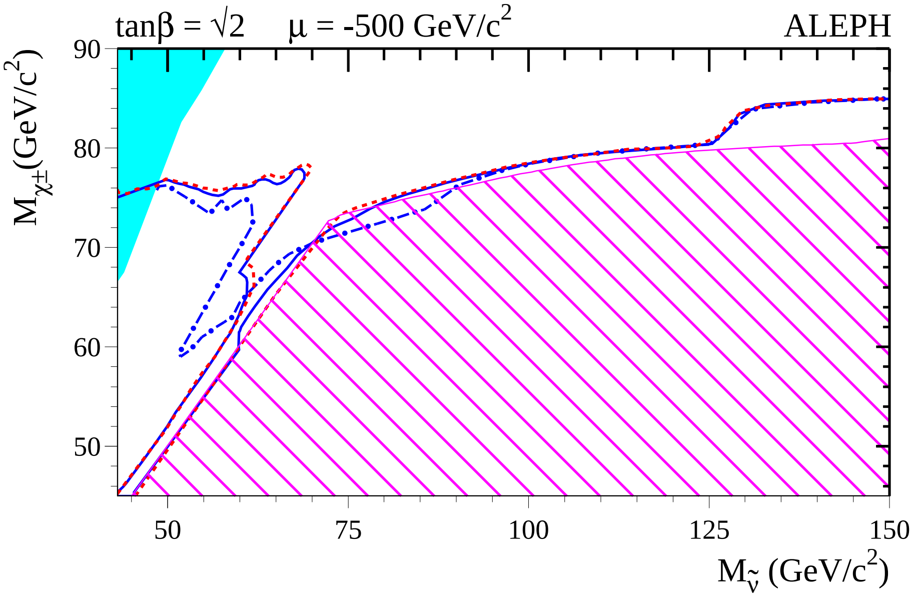

Figure 10: *The limit on the chargino mass as a function of sneutrino mass, for* $\mu = -500\ \mathrm{GeV}/c^2$*,* $\tan\beta = \sqrt{2}$*, and various* A_τ*. First, a universal scalar mass is assumed, and the limit is derived for* $A_\tau = 0$ *(solid curve),* $A_\tau = +1\ \mathrm{TeV}/c^2$ *(dashed curve) and* $A_\tau = -1\ \mathrm{TeV}/c^2$ *(dot-dash curve). Second, the assumption of a universal* m_0 *is dropped, and the impact of stau mixing is maximised (for three-body chargino decays), shown as the hatched region. The shaded region at low* $M_{\tilde{\nu}}$ *is theoretically forbidden for* $A_\tau = -1\ \mathrm{TeV}/c^2$*.*

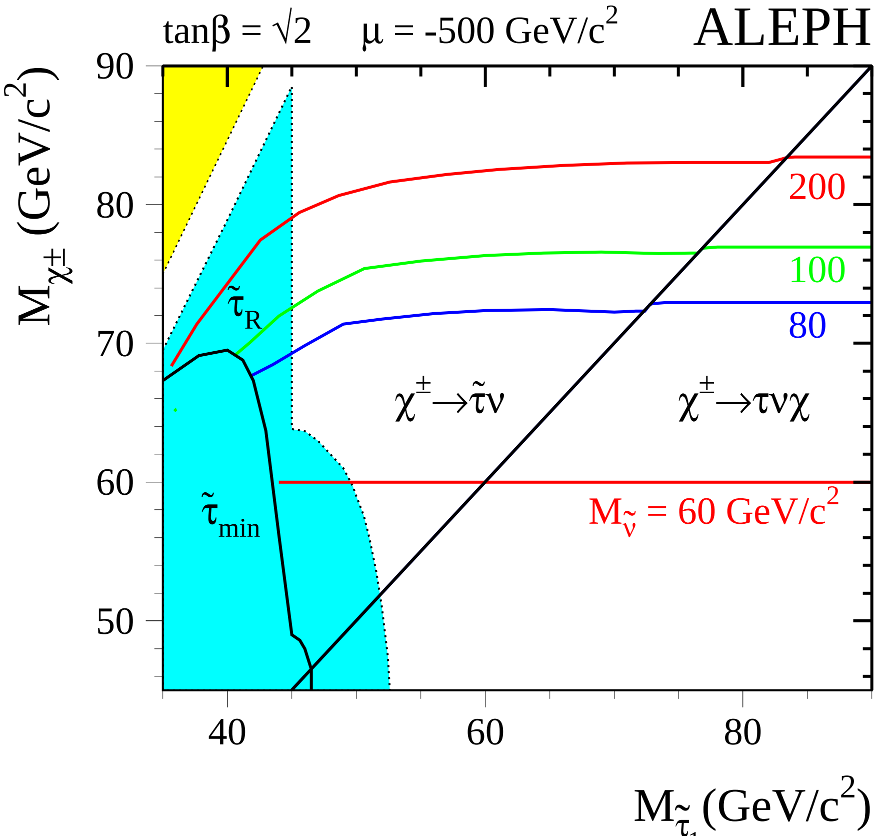

Figure 11: *The limit on the chargino mass as a function of stau mass, for several values of the sneutrino mass, for* $\mu = -500\ \mathrm{GeV}/c^2$ *and* $\tan\beta = \sqrt{2}$*. The limits from direct searches for staus [2] are also indicated, where the area labelled* $\tilde{\tau}_R$ *is excluded for pure right-staus, and the area labelled* $\tilde{\tau}_{\min}$ *is the most conservative limit. The light shaded triangular region in the upper left corner corresponds to* $M_\chi > M_{\tilde{\tau}_1}$ *and is not considered here.*

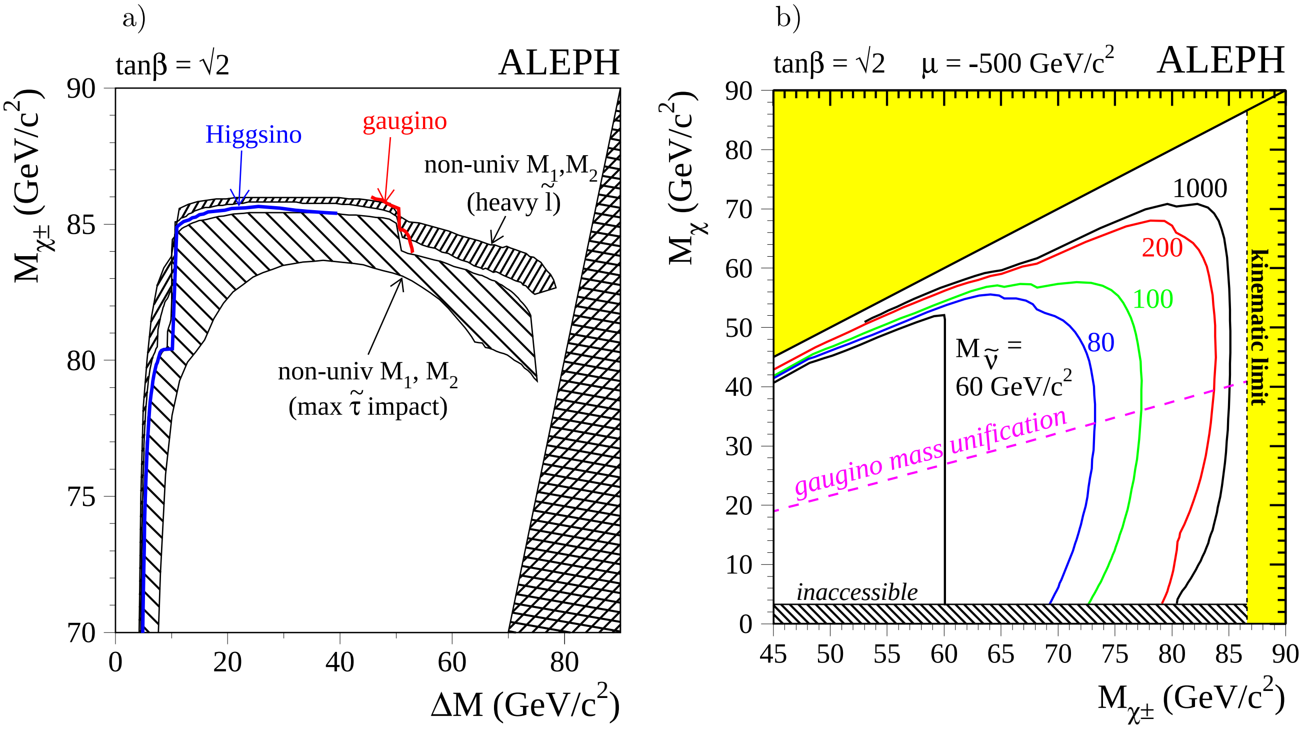

Figure 12: *a) The limit on the chargino mass as a function of* ΔM*, for* $M_{\tilde{\nu}} \geq 200$ GeV/c^2*. The thick solid curves indicate the limit in the Higgsino and gaugino regions, assuming gaugino mass unification. The hatched regions reflect the spread in the limits if gaugino mass unification is relaxed, as* μ *is varied from* -80 *to* -500 GeV/c^2*, for heavy sleptons, and maximising the impact of stau mixing. b) The limit in the* $(M_{\chi^\pm}, M_\chi)$ *plane, relaxing gauge unification relations for the gaugino and slepton masses, for several values of* $M_{\tilde{\nu}}$*. The dashed curve indicates the limit if the gaugino mass unification relation is assumed. The inaccessible region for very low* M_χ *can not be attained by relaxing the gauge unification relation.*